Chapter 6
Monsoon Dynamics and Its Interactions with Ocean

Abstract In this chapter, the basic concept of the monsoon is introduced, followed by the discussion of monsoon variability on the quasi-biennial and lower-frequency timescales. The mechanisms responsible for the tropospheric biennial oscillation (TBO) and the monsoon – warm ocean interaction – are discussed. Next, how the ENSO affects the monsoon variability over East Asia and South Asia and how the remote and local SST anomalies affect western Pacific circulation anomalies are discussed. Finally, the physical mechanisms responsible for the in-phase and out-of-phase relationships among the Indian monsoon, western North Pacific monsoon, and Australian monsoon are discussed.

6.1 Introduction

The original meaning of the monsoon was derived from an Arabic word for season. The monsoon is characterized by the seasonal reversal of prevailing wind direction. Figure 6.1 shows large-scale surface wind and pressure patterns in northern winter and summer. In northern winter, the southern hemisphere surface receives more shortwave radiation. As a result, high pressure controls the Eurasian continent, and there is an anticyclonic flow around the continent due to the rotation of Earth. Southward cross-equatorial flows converge onto the ITCZ south of the equator over the Indian Ocean and the Australian monsoon region. In northern summer, the surface pressure and wind in general reverse sign, with low-pressure center and cyclonic flow located over the Eurasian continent and northward cross-equatorial wind over the Indo-western Pacific sector. Thus, the seasonal change of land–ocean thermal contrast in response to solar forcing is a major driver for the generation of the monsoon. Because Eurasia contains the largest land mass and the highest mountains in the world, Asian monsoon becomes the most powerful monsoon system in the Earth.

The classic definition of the monsoon was based on the reversal of the seasonal wind, but such a definition may include high-latitude regions. Thus, it is proper to consider the seasonal change of rainfall. In addition to land–ocean thermal contrast, the monsoon can be also driven by hemispheric asymmetric SST gradient. In this regard, a concept of oceanic monsoon is introduced, to differentiate it from the classic "continent monsoon." Furthermore, due to the thermal forcing of the

T. Li, P.-c. Hsu, *Fundamentals of Tropical Climate Dynamics*,
Springer Atmospheric Sciences, DOI 10.1007/978-3-319-59597-9_6

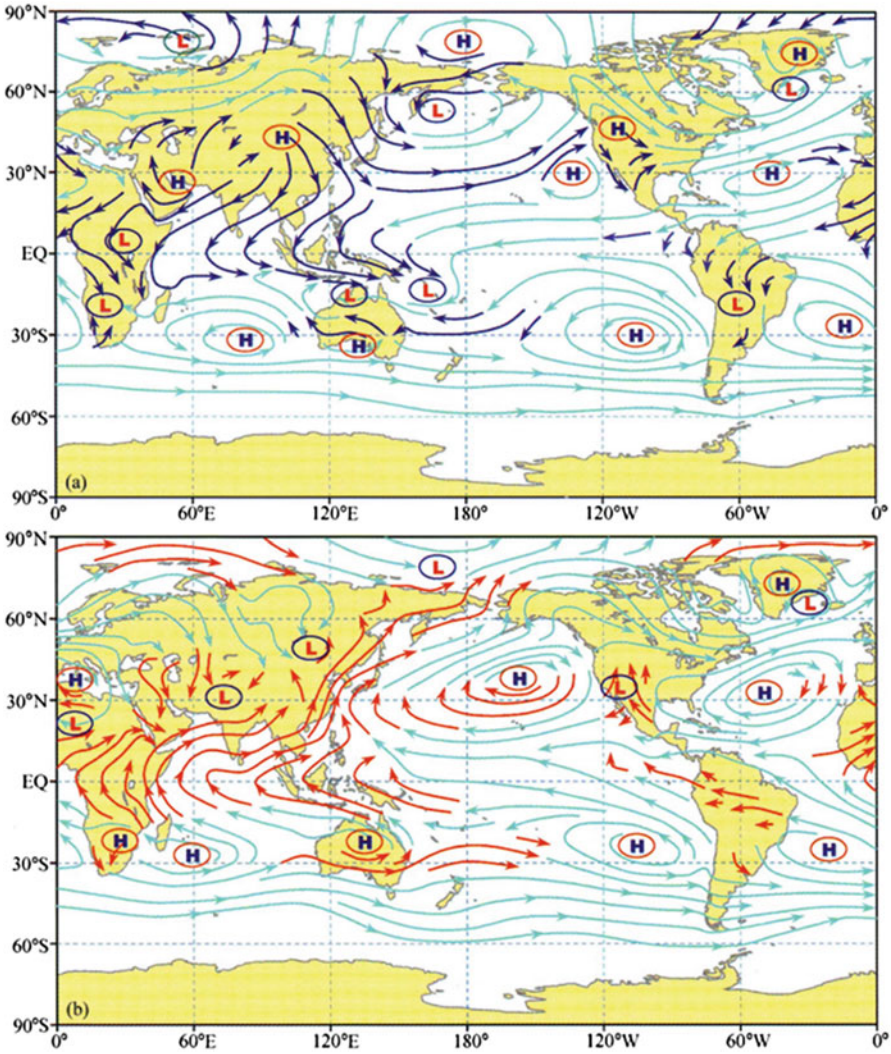

Fig. 6.1 Schematic of global surface pressure and wind patterns in northern winter (DJF) and northern summer season (JJA)

Tibetan Plateau, the monsoonal flow can penetrate into mid-latitudes. In this regard, a new concept of subtropical monsoon is introduced.

Base on the above consideration, the Asian monsoon system is further separated into three subcomponents, namely, Indian monsoon (IM), East Asian monsoon (EAM), and western North Pacific monsoon (WNPM). Figure 6.2a shows the domain of the three sub-monsoon systems (Wang et al. 2003a, b) based on the characteristics of summer–winter precipitation and low-level wind difference fields. As seen from this figure, IM is characterized by lower-level westerlies and

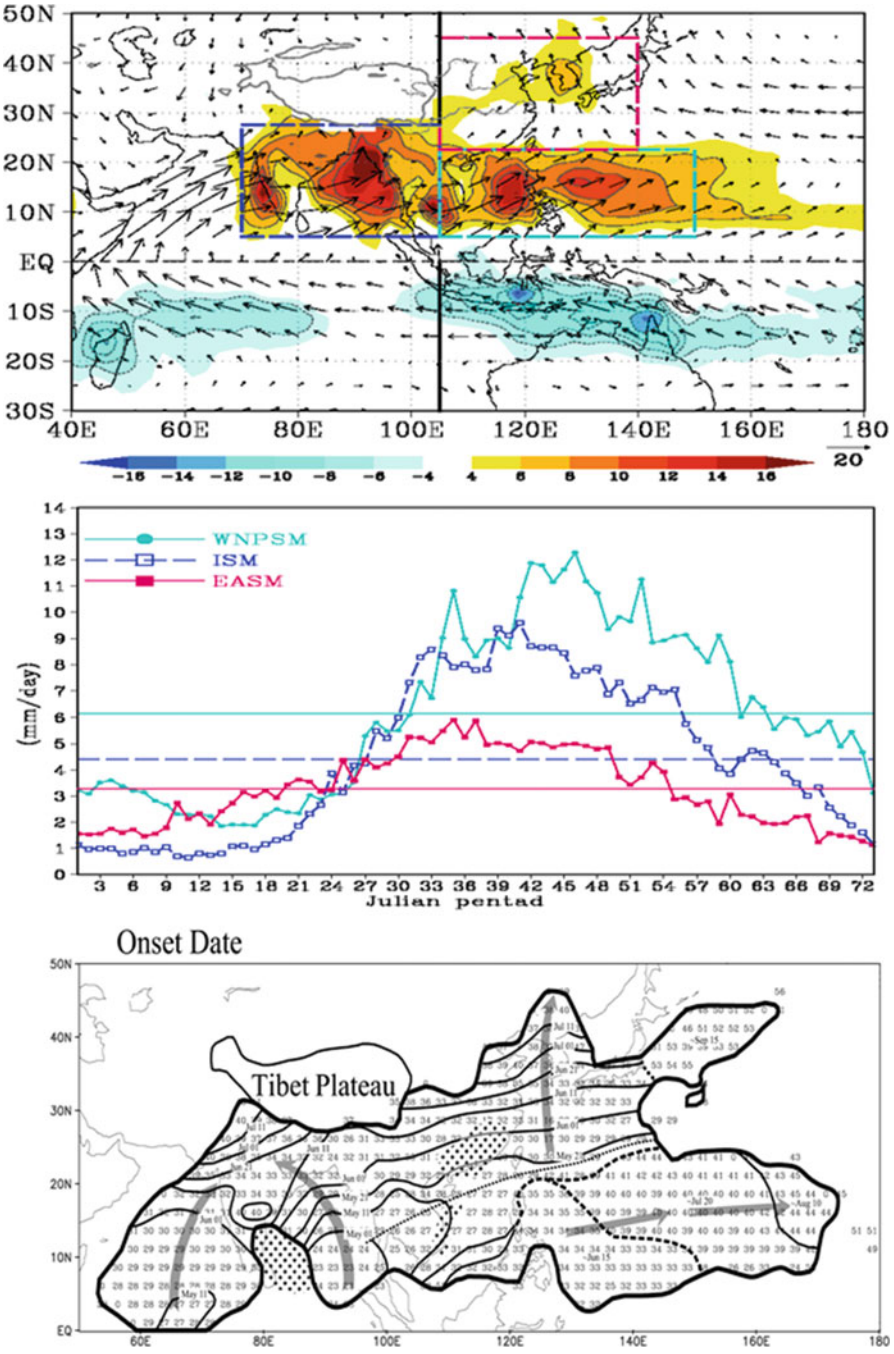

Fig. 6.2 The domain of IM, WNPM, and EAM and rainfall (shading) and 850-hPa wind (vector) difference fields between July–August and January–February (*top panel*, from Wang et al. 2003a), the climatological pended rainfall evolution averaged over the IM, WNPM, and EAM boxes (*middle panel*, from Wang et al. 2003a) (Copyright © 2003 Elsevier B. V. All rights reserved). (*Bottom*) climatological onset date for the Asian monsoon region (From Wang and LinHo (2002). © Copyright 2002 American Meteorological Society (AMS))

upper-level easterlies, being in a thermal wind relation with a north–south thermal contrast between the heated Asian land and cool Indian Ocean, while EAM has pronounced lower-level southerlies in association with the east–west thermal contrast between the Asian continent and mid-latitude Pacific Ocean. Whereas IM and EAM are typical continental monsoons driven by land–ocean thermal contrast, WNPM is an oceanic monsoon driven primarily by hemispheric asymmetric SST gradients.

Figure 6.2b shows climatological annual rainfall evolution averaged over the three equal-area boxes. The strength of the three sub-monsoon systems is distinctive, with greatest (least) total rainfall amounts occurring in the WNPM (EAM) region. The time evolution of the Asian monsoon has distinctive regional characteristics (Fig. 6.2c). The convection first develops over the Bay of Bengal (BOB) in late April. After that, the monsoon is triggered over the South China Sea (SCS) and then moves northward to East Asia. EAM is normally referred to as a subtropical monsoon encompassing eastern China, Japan, Korea, and adjacent marginal seas and monsoon oceans, i.e., the area between 20° and 45°N and from 100° to 140°E. The major rain-producing system is the monsoon subtropical front, which is also known as Meiyu or Baiu front during early summer when it is located along the Yangtze River valley extending to southern Japan. The Meiyu is preceded by the onset of the SCS summer monsoon, which, on average, occurs in mid-May when heavy convective rainfall suddenly develops over the northern SCS and westerly flows control the central SCS (e.g., Wang and Wu 1997; Xie et al. 1998; Lau and Wu 2001). The SCS onset is first followed by an establishment of a rainband over the northwest flank of the WNP subtropical high extending from the southern coast of China, to Taiwan, to east of Okinawa. Around June 10, the EAM front and associated rainband move rapidly northward to the Yangtze River valley and southern Japan, where continuous rain and cloudiness last for about a month. In mid-July the rain belt further advances northward to northern and northeast China. In late August, the EASM begins to withdraw southward in northern China. The sub-seasonal stepwise progression of the EAM rainband is one of the features distinctive from IM. During the IM period, the convective rainband gradually moves northward from BOB and Arabian Sea from early May to July. WNPM, on the other hand, is characterized by the eastward propagation of convective rainbands from middle May to August.

In addition to a remarkable annual cycle, the Asian monsoon also exhibits a strong intraseasonal oscillation (ISO) in both rainfall and circulation fields. ISO was first detected by Madden and Julian (1971), who found a significant period of 40–50 days in the zonal wind field over the Canton Island. Later they further found that this oscillation is of global scale and is characterized primarily by equatorial eastward propagation with a zonal wave number-one structure (Madden and Julian 1972). While the eastward propagating ISO mode is primarily observed in boreal winter, ISO in boreal summer is dominated by northward propagation in the Asian monsoon region. In Chap. 3 we discuss the physical mechanisms responsible for the northward propagation. The northward propagation is primarily found

over northern Indian Ocean and South China Sea regions, while the westward propagation of ISO is found in the off-equatorial tropical western North Pacific.

Observations show that the intraseasonal variation of the rainfall over the South Asian monsoon region is closely linked to the northward propagation of BSISO. Figure 6.3 illustrates the total variance of the boreal summer ISO (BSISO) over a 20-year period and area-averaged rainfall evolution over Indian subcontinent in 2004. It is worth noting that the amplitude of the intraseasonal rainfall variation over the Indian monsoon region is comparable to that of the annual cycle. This indicates that even within the monsoon season, rainfall change can be quite large. From May to October 2004, Indian rainfall experienced six major active phases, and each phase or peak corresponds well to a northward-propagating ISO. Given such a close relationship, forecasting the active and break phase of the Indian monsoon becomes possible, as long as that the model is able to capture the northward-propagation of ISO.

Besides the strong intraseasonal variability, the Asian monsoon also experiences a significant year-to-year change. Among many factors, El Niño–Southern Oscillation (ENSO) has been considered as a major forcing factor that regulates the interannual monsoon rainfall variability. Walker (1923, 1924) first recognized the effect of the Southern Oscillation on IM. Since then, a number of studies have been conducted to elucidate the monsoon–ENSO relationship (e.g., Yasunari 1990; Webster and Yang 1992; Ju and Slingo 1995; Lau and Yang 1996; see Webster et al. 1998 for a review). IM tends to have a simultaneous negative correlation with the eastern Pacific SST. The physical process through which ENSO impacts the IM is through the modulation of convective heating over the Maritime Continent (MC), which further induces low-level anticyclonic circulation to its northwest as a Rossby wave response (Gill 1982). The summer mean flow (e.g., easterly vertical shear) further modulates this anomalous Rossby wave response (Wang et al. 2003a, b). In addition to the external forcing from ENSO, monsoon–ocean interaction itself in the warm pool may support a natural quasi-biennial mode, and this mode is named as the tropospheric biennial oscillation (TBO). In the subsequent sections, we will first introduce TBO, followed by the monsoon–ENSO interaction.

6.2 Theories on Tropospheric Biennial Oscillation (TBO)

Observed all-Indian rainfall time series (climatological mean removed) shows a clear quasi-biennial signal (Fig. 6.4a). Surprisingly, such a rainfall fluctuation is highly correlated to ocean subsurface temperature change thousands of miles away in the equatorial western Pacific. This observed relationship implies that active ocean–atmosphere interactions that happen in the vast are of the warm pool on the quasi-biennial timescale. Figure 6.4b illustrates the power spectrum of the all-Indian rainfall index during 1949–1998. Note that different from the Niño 3 index that has a maximum power-spectrum peak at 3–4 years, the monsoon

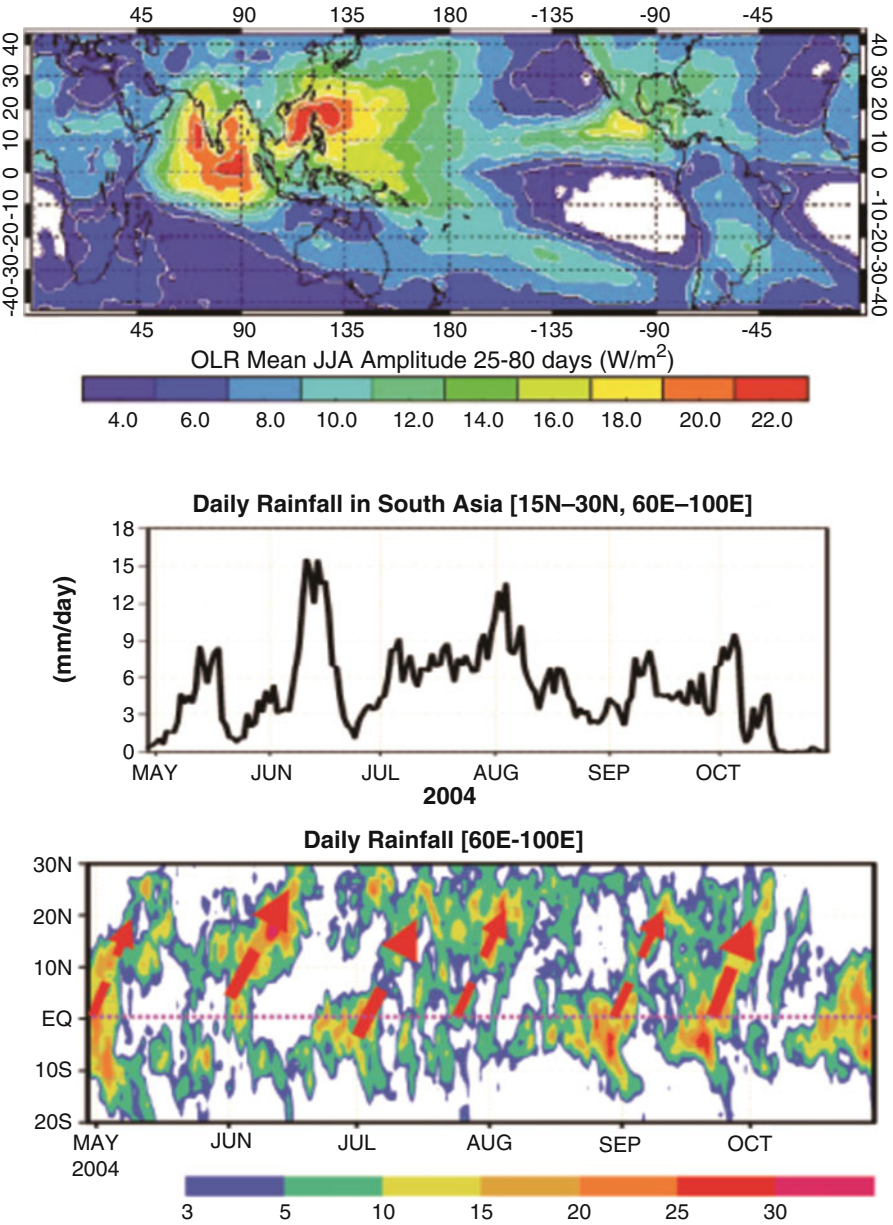

Fig. 6.3 Standard deviation of 25–80-day filtered OLR fields for the period of 1981–2002 (*top panel*), time evolution of 2004 daily rainfall averaged over South Asia (15°–30°N, 60°–100°E) (*middle panel*), and the latitude-time section of the 2004 daily rainfall along 60°–100°E (*bottom panel*)

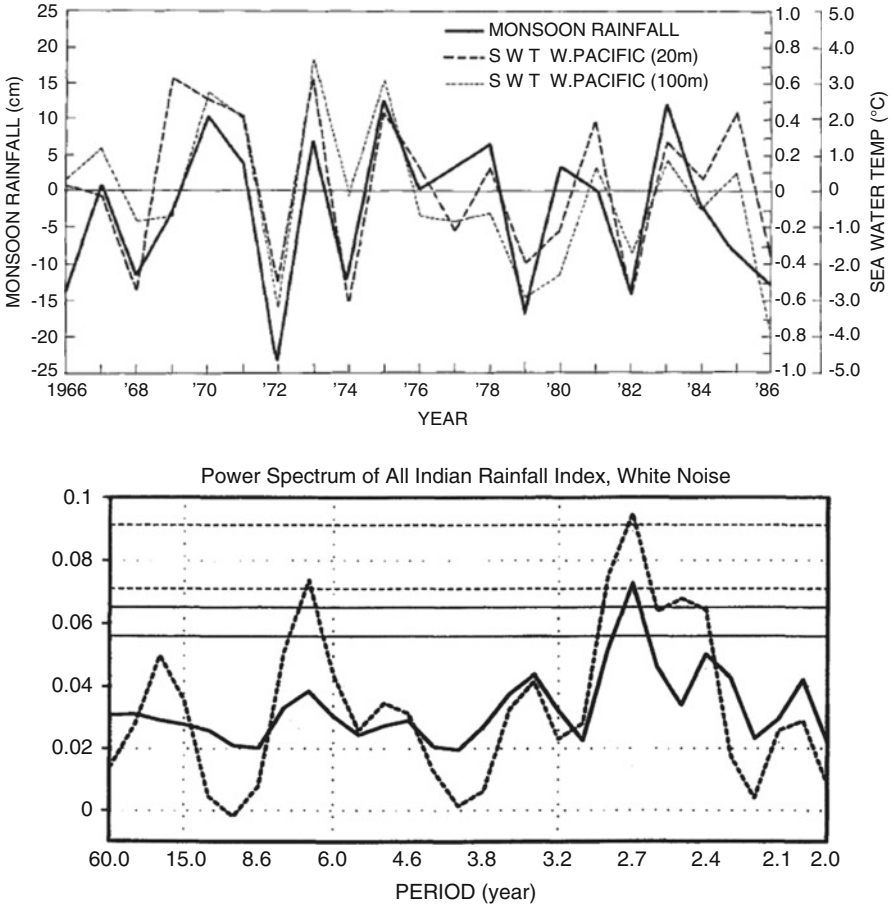

Fig. 6.4 (*Top*) Time series of anomalous all-Indian rainfall and ocean temperature anomalies at 20-m and 100-m depth over equatorial western Pacific (From Yasunari 1990). (*Bottom*) Power spectrum of all-Indian rainfall index during 1949–1998 (From Li et al. 2001. © Copyright 2001 American Meteorological Society (AMS))

exhibits a strongest peak at the quasi-biennial (2–3 years) period. The observational facts above indicate the quasi-biennial nature of the monsoon.

The tendency of the rainfall anomaly to "flip-flop" in successive years is referred to as the tropospheric biennial oscillation (TBO, Meehl 1994, 1997). Observations show that TBO is manifested over various monsoon regions such as Indonesia/Northern Australia (Nicholls 1978; Yasunari and Suppiah 1988), East Asia/WNP (Lau and Sheu 1988; Tian and Yasunari 1992; Shen and Lau 1995; Chang et al. 2000a, b; Wang and Li 2004; Li and Wang 2005), and India (Mooley and Parthasarathy 1984; Meehl 1987; Rasmusson et al. 1990; Yasunari 1990, 1991).

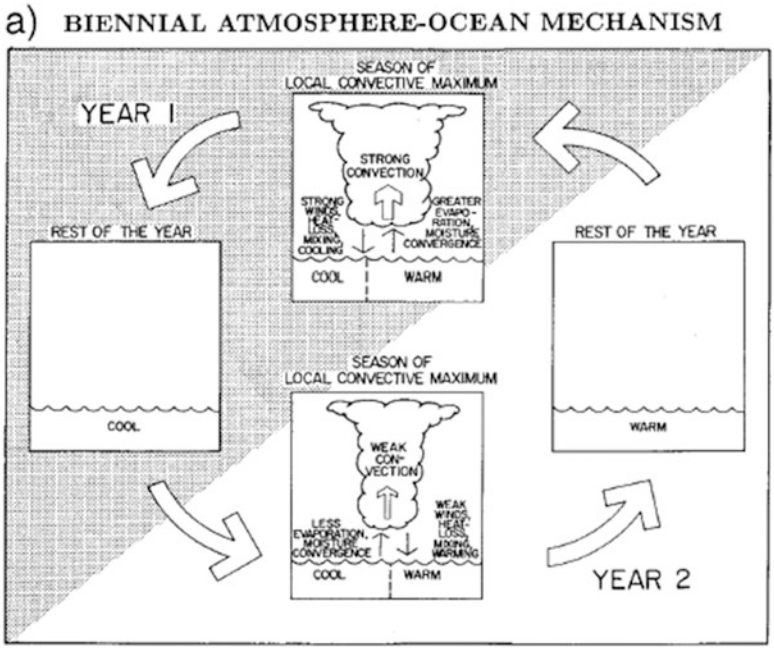

Fig. 6.5 A schematic diagram illustrating a local atmosphere–ocean interaction mechanism for generating a biennial oscillation (From Meehl (1993). © Copyright 1993 American Meteorological Society (AMS))

Why does the monsoon favor the quasi-biennial variability? So far three theories have been put forward in an attempt to understand the origin of the TBO. The first theory emphasizes local air–sea interaction (Nicholls 1978; Meehl 1987). Figure 6.5 is a schematic diagram illustrating essential processes responsible for the TBO. Because of circular argument, one may start from any time point. Suppose we start from a strong monsoon season. Due to strengthened monsoon, surface wind and convective clouds are both enhanced. This leads to enhanced surface evaporation and reduced shortwave radiation into the ocean. Thus, the ocean surface cools. Assume the cooling of the ocean can last for three seasons till the onset of the next monsoon due to long ocean memory. The cooler ocean next summer would lead to a weaker monsoon. The weakened monsoon leads to weakened surface wind and less clouds, which can warm the ocean through reduced surface evaporation and enhanced downward shortwave radiation. The warming may last three inactive seasons to impact the monsoon intensity in the following year. Through this local air–sea feedback process, a biennial oscillation is generated.

The second theory involves inter-basin teleconnection between tropical Indian Ocean and western Pacific and Indian and Australian monsoon interaction with surrounding oceans (Chang and Li 2000; Li et al. 2006). A simple five-box model was constructed, to understand the observed Indian monsoon – Australian monsoon in-phase relationship (Fig. 6.6). A warm SSTA over tropical Indian Ocean favors a

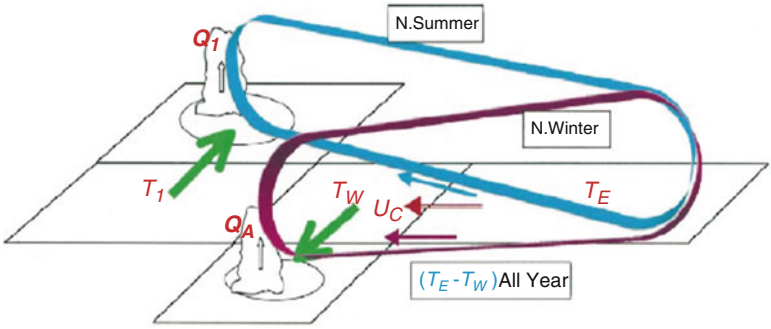

Fig. 6.6 Schematic diagram from a five-box model with T_I and $\mathbf{T_W}$ denoting SST over tropical Indian Ocean and Maritime Continent/western Pacific, Q_I and Q_A denoting heating over Indian monsoon and Australian monsoon regions, the eastern box denoting tropical eastern Pacific (From Chang and Li (2000). © Copyright 2000 American Meteorological Society (AMS))

strengthening of the Indian monsoon through enhanced moisture transport. The strengthened monsoon induces a large-scale east–west circulation and thus an easterly anomaly over the Maritime Continent, the latter of which further warms the SST in the region in the subsequent season as the anomalous wind is against the mean westerly. The SST warming over the Maritime Continent north of Australia further strengthens the Australian monsoon. The strengthened Australian monsoon induces westerly anomalies over the equatorial Indian Ocean, which may cool the ocean through both the increase of the surface evaporation (because mean wind is westerly) and cold zonal advection. The cooling of the tropical Indian Ocean would lead to the weakening of the Indian monsoon in the subsequent summer. Through this inter-basin teleconnection, a biennial oscillation is generated for both the Indian and Australian monsoon, and an enhanced Australian monsoon always follows an enhanced Indian monsoon.

To test the hypothesis that the ocean–atmosphere interactions in the monsoon/warm ocean region may lead to the TBO, Li et al. (2006) conducted idealized numerical experiments of a hybrid coupled atmosphere–ocean GCM. The atmospheric component of this hybrid coupled model is the ECHAM4 T30L19 version. The ECHAM4 has been coupled to an intermediate ocean model (Wang et al. 1995) without a heat flux correction (e.g., Fu et al. 2002, 2003). The intermediate ocean model consists of two active layers of the upper ocean, a mixed layer with variable depth, and a thermocline layer overlying an inert deep ocean (Wang et al. 1995). The latest version of the model combines the upper-ocean dynamics described in McCreary and Yu (1992) and the mixed-layer physics (Gaspar 1988). The model has a self-contained parameterization scheme for entrained water temperature that considers influences on entrained water temperature from both the thermocline displacement and the mixed-layer temperature (Wang et al. 1995). The effects of shear production, wind stirring, and buoyancy forcing are included in the vertical entrainment velocity calculation. The model has the capability of simulating

realistic annual cycle and interannual variations of SST, thermocline depth, and mixed-layer depth (Fu and Wang 2001).

To explore the role of the atmosphere–warm ocean interaction, Li et al. (2006) designed an idealized hybrid coupled GCM experiment in which the atmosphere and ocean are coupled only in the tropical IO and western Pacific (30°S–30°N, 40°E–180°E), while the climatological monthly mean SST is specified elsewhere. By doing so, we exclude the effect of the remote El Niño forcing.

After initial 10-year spin-up, the coupled model was integrated for 50 years. The long-term simulation shows that the coupled model is capable of simulating realistic annual cycle and ENSO-like interannual variability in the equatorial Pacific. The seasonal mean SST errors are in general smaller than 1 °C in the most of the ocean domain except near the coast of North Africa in boreal summer and the coast of west Australia and SCS in boreal winter.

The diagnosis of standard deviation of the total interannual (1–8-year) variability of the model SST and the relative strength of the quasi-biennial (QB, 1.5–2.5-year) component reveals that the greatest interannual SST variabilities appear in the BOB, southeast Indian Ocean (SEIO), WNP, and SPCZ, where the biennial component is also largest. The averaged ratio of the biennial SST variability in the four regions exceeds 60%, about a factor of two larger than the observed, indicating that in this model configuration without the eastern tropical Pacific, the TBO is a dominant signal. Strong TBO signals also appear in the middle-tropospheric (500 mb) vertical motion and low-level (850 mb) zonal and meridional wind components. The power spectrums of the time series of the model SST and 500 mb vertical velocity show that the TBO peaks, ranged from the period of 20–28 m, clearly appear in these spectrums, and they exceed a 95% significance level. The results suggest that the monsoon–warm ocean interaction favors a pronounced biennial variability.

To illustrate the spatial pattern and evolution characteristics of TBO in the Indo-Pacific warm ocean region, a season-sequence EOF analysis is performed for both the model and the NCEP reanalysis. Figure 6.7 illustrates the seasonal evolution of 850mb wind and 500mb vertical p-velocity fields in the model. Here, the vertical velocity has been multiplied by −1 so that a positive value in Fig. 6.7 represents an enhanced rainfall anomaly. It is noted that the model in general captures the gross structure and evolution patterns of the observed TBO in the region. For instance, in JJA(0), the circulation anomaly in the SEIO is characterized by downward motion (or suppressed convection) and anticyclonic low-level flows, while in the WNP, it is characterized by cyclonic flows and upward motion. The SEIO anticyclone is pronounced in northern fall and decays in subsequent seasons. Subsidence motion and anticyclonic flows develop over the Philippines and SCS in SON(0), and they shift slightly eastward in subsequent seasons and persist until JJA(1). The circulation anomalies in JJA(1) have an opposite polarity relative to those in the previous summer.

Since the model does not contain the ENSO mode, the model TBO arises solely from air–sea interactions in the Indo-Pacific warm ocean region. What are specific processes that give rise to the TBO variability in this region? Figure 6.8 illustrates

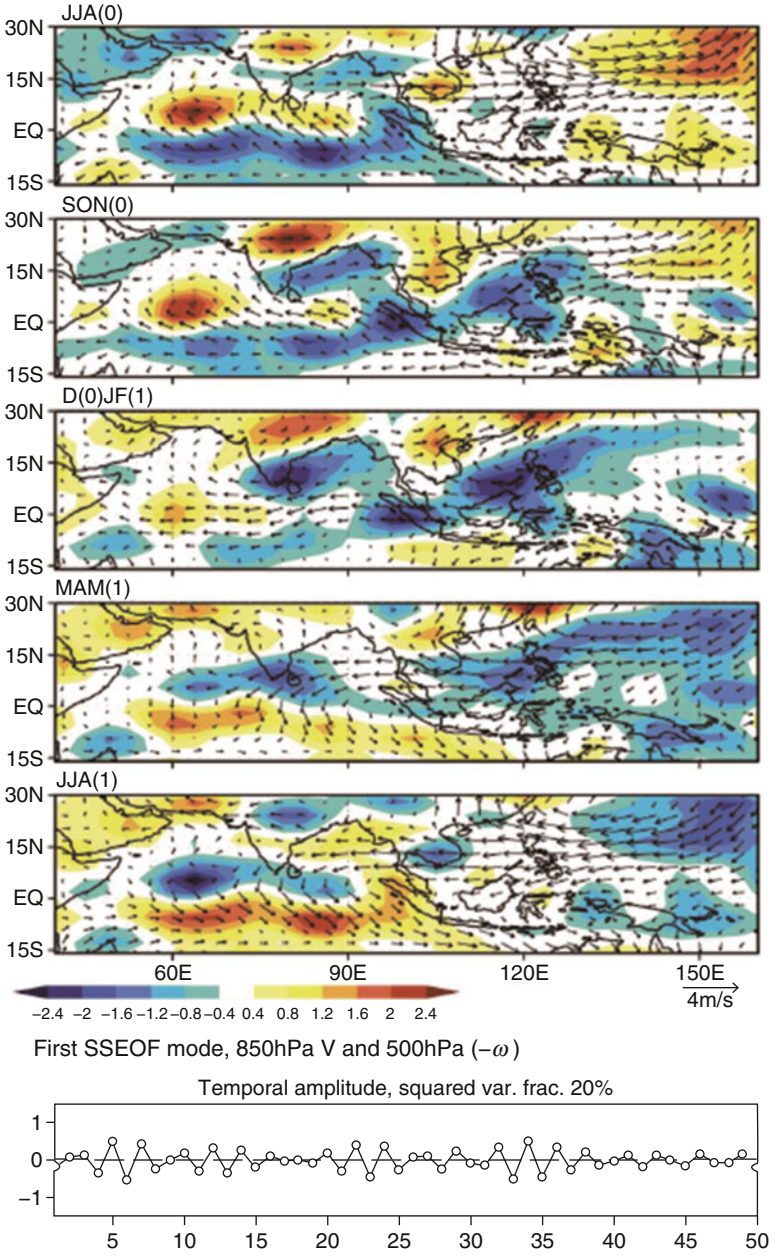

Fig. 6.7 Seasonal evolution of 500 hPa vertical p-velocity (*color shaded*; units, Pa/s) and 850 hPa wind anomaly (vector) associated with the TBO obtained from a season-sequence EOF analysis of 50-year. output of the hybrid coupled GCM (Li et al. 2006). The time coefficient of the SSEOF mode is shown in the *bottom panel*. The vertical velocity has been multiplied by −1 so that positive contours represent enhanced convection anomalies (From Li et al. (2006). © Copyright 2006 American Meteorological Society (AMS))

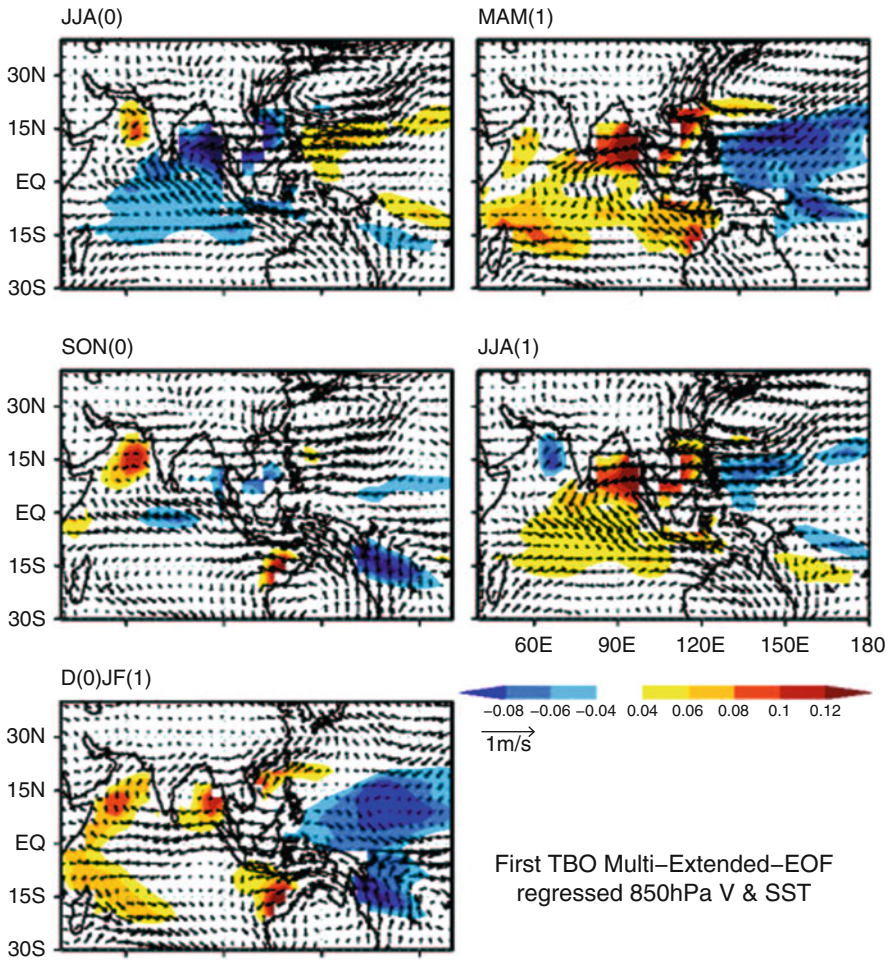

Fig. 6.8 Same as Fig. 6.7 except for the regressed SST (*shading*; unit, K) field from the hybrid coupled GCM (Form Li et al. (2006). © Copyright 2006 American Meteorological Society (AMS))

the seasonal evolution pattern of the SSTA, which is regressed based on the time coefficient of the first SS-EOF mode. A significant surface cooling occurs in JJA (0) in the eastern IO and off the Asian coast, with maximum cold SSTA appearing in BOB and SCS. While the cold SSTA decays in subsequent seasons, new cold SST anomalies develop in the western Pacific in SON(0) and DJF(1). In particular, the cold SSTA in the WNP reaches a peak in DJF(1) and persists for 2–3 seasons till the following summer, JJA(1), when the SSTA in the eastern IO and SCS has completely reversed sign from a cold to a warm anomaly.

The diagnosis of the model SST budget reveals that the cooling in the IO in JJA (0) is primarily attributed to the surface evaporation and vertical ocean mixing due to enhanced surface wind speeds, whereas the cooling in the western Pacific in SON

(0) and DJF(1) is mainly attributed to the ocean dynamic processes in response to anomalous wind stress curl (see discussions below). Based on the model circulation and SST evolution, a hypothesis is put forth to explain the TBO in the model. Assume we start from a strong WNP monsoon in JJA(0). In response to enhanced WNP monsoon heating, northward low-level cross-equatorial winds are generated. The anomalous winds enhance the seasonal mean winds, leading to increased surface evaporation and ocean vertical mixing and thus negative SSTA in the eastern IO and off the Asian coast. It is seen from Fig. 6.8 that the strongest SST cooling appears in the BOB, SCS, and MC. This SST cooling has a significant impact on the strength of the annual convective maximum that migrates to Southeast Asia in SON and MC in DJF (Meehl 1987). The so-induced suppressed convection in SCS and MC may further induce anomalous westerlies over the equatorial western Pacific through anomalous Walker circulation.

The curl of the zonal wind stress anomaly near the equator may exert a dynamic impact on SST by exciting upwelling oceanic Rossby waves and by lifting the ocean thermocline. As a result, the ocean surface cools. The diagnosis of the mixed-layer heat budget in the ocean model confirmed that the negative SST tendency in the western Pacific in SON(0) and DJF(1) is indeed attributed to the ocean dynamics terms (i.e., 3D ocean temperature advection), while the net heat flux effect is modest, particularly in DJF(1).

The cold SSTA over the WNP, once initiated by the ocean dynamics, may persist from northern winter to the following summer through the positive thermodynamic air–sea (TAS) feedback proposed by Wang et al. (2000). The persisted cold SSTA eventually leads to suppressed convection and thus a weaker WNP monsoon in JJA (1), thus completing a TBO transition from a local cyclonic circulation in JJA(0) to an anticyclone in JJA(1). The weakened WNP monsoon induces southward cross-equatorial flows, leading to anomalous ocean surface warming in the eastern IO and SCS, and thus the second half of the TBO cycle begins in this region.

Figure 6.9 is a flow chart that illustrates key physical processes that causes the TBO in the hybrid coupled GCM. Starting from a strong WNP monsoon in boreal summer, the strong convection in the WNP causes strong northward cross-equatorial flows. The anomalous winds induce cold SSTA in the SCS, MC, and SEIO off Sumatra, leading to suppressed convection in the MC through either a local SSTA impact on the seasonal convective maximum or its effect in surface wind divergence/moisture and local Walker circulation over the IO. The suppressed convection in the MC induces anomalous westerlies in the western Pacific, which further lead to a cold SSTA in the WNP through either a direct ocean dynamic effect (via ocean Rossby waves and thermocline changes) or an indirect atmospheric effect (through the central-eastern equatorial Pacific heating and associated atmospheric Rossby wave response). The so-induced cold SSTA in the WNP persists through the TAS feedback and leads to the weakening of the WNP monsoon in the following summer. Thus, the second half cycle of the TBO begins. This confirms earlier hypotheses that the biennial component of ENSO is a part of TBO, resulting from teleconnections between the tropical Pacific and Indian Oceans.

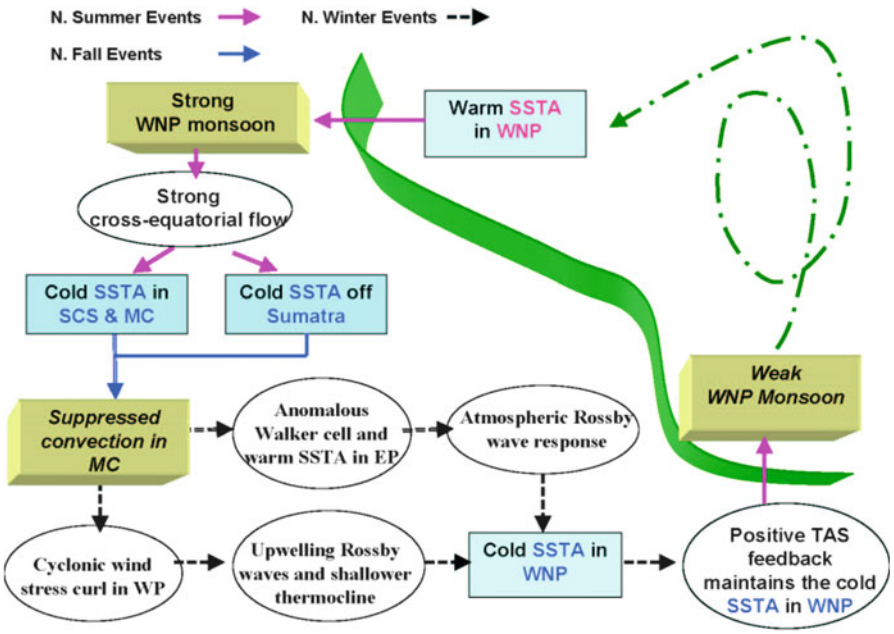

Fig. 6.9 A schematic diagram illustrating essential processes that lead to the TBO in the tropical Pacific and Indian Oceans. The *left* part of a *green ribbon* consists of a half of the TBO cycle, which starts from a strong WNP summer monsoon at year 0 and ends to a weak monsoon at year 1. The *red*, *blue*, and *black arrows* indicate, respectively, northern summer, fall, and winter events (From Li et al. (2006). © Copyright 2006 American Meteorological Society (AMS))

The third theory involves a tropical–mid-latitude interaction (Meehl 1997). Based on a model diagnosis, Meehl (1997) suggested tropical heating anomalies associated with strengthened monsoon may exert a remote forcing in mid-latitude circulation in such a way that it reduces land–ocean thermal contrast over the Asian Continent–Indian Ocean sector and promotes a weakened monsoon in the following summer. However, given the chaotic nature of mid-latitude circulation, how teleconnection patterns associated with tropical forcing can persist through a few seasons is a key issue that needs to be resolved.

6.3 Quasi-Biennial and Lower-Frequency Variability of the Monsoon

The power spectrum of the time series of the domain-averaged India rainfall reveals that on interannual timescales, there are two distinctive peaks (bottom panel of Fig. 6.4), with the quasi-biennial (QB) component [2–3 years, hereafter referred to as the monsoon QB mode or tropospheric biennial oscillation (TBO) mode] being

much greater than the lower-frequency (LF) component [3–7 years, hereafter referred to as the monsoon LF mode]. The similar two power-spectrum peaks also appeared in the first EOF mode of the global precipitation field (Lau and Sheu 1988) and in the meridional wind over the South China Sea and sea-level pressure difference between the Asian continent and Northwestern Pacific (Tomita and Yasunari 1996). Webster et al. (1998) investigated the temporal characteristics of the Indian monsoon rainfall variability by the use of a wavelet analysis and found the intermittent recurrence of the two power-spectrum peaks. The Niño 3 SST anomaly (SSTA) also has two significant spectrum peaks, but its LF component is much greater than its QB component. Natural questions that need be addressed are why the Indian monsoon has a more pronounced QB spectrum peak and what physical mechanisms are responsible for the monsoon variability on both the timescales.

In this section we discuss the physical mechanisms responsible for the QB and LF variability of the Indian monsoon rainfall by revealing the spatial and temporal structures of atmospheric circulation and SST associated with the two modes. Our strategy is first to apply a time-filtering technique to separate rainfall data into 2–3-year and 3–7-year bands, respectively. Then, by analyzing the spatial and temporal patterns of atmospheric circulation associated with the two bands, we intend to investigate physical processes responsible for the rainfall variability on the two timescales. To compare with results from the time-filtering analysis, we will also conduct a composite analysis using the original unfiltered data.

The primary data used in this study are the domain-averaged Indian rainfall; NCAR/NCEP reanalysis that includes wind, moisture, temperature, and geopotential height fields; and the Reynolds SST (Reynolds and Smith 1994) for a period of 1949–1998. The Indian rainfall is represented by an area-averaged precipitation from 26 stations reasonably distributed over the Indian subcontinent. These gauge stations are picked up from the NOAA climatological baseline station data over land, documented at NCDC, and updated from CAC global CEAS summary of day/month observations. This area-averaged rainfall has a correlation coefficient of 0.86 with the all-Indian rainfall index (Mooley and Parthasarathy 1984).

A band-pass filter (Murakami 1979) is used to separate the data into approximately 2–3-year and 3–7-year windows, respectively. These two bands represent the two significant power-spectrum peaks in the area-averaged Indian rainfall field. A lagged correlation analysis is then performed for each dataset. A composite analysis using the original unfiltered data is also carried out to crosscheck the lagged correlation analysis results obtained from the time-filtered data.

Figure 6.10 shows the lagged correlation between the Indian summer rainfall and domain-averaged SSTs in the Indian Ocean (IO, 60°–95°E and 0°–15°N), western Pacific (WP, 130°–150°E and 10°–20°N), and eastern Pacific (EP, 170°–120°W and 5°S–5°N). In the 2–3-year band (top panel), a significant positive correlation between the IO SSTA and the monsoon rainfall appears in the preceding winter and spring, with a maximum correlation coefficient exceeding 0.6, far above the 95% significance level. (The 95% level corresponds to a correlation coefficient

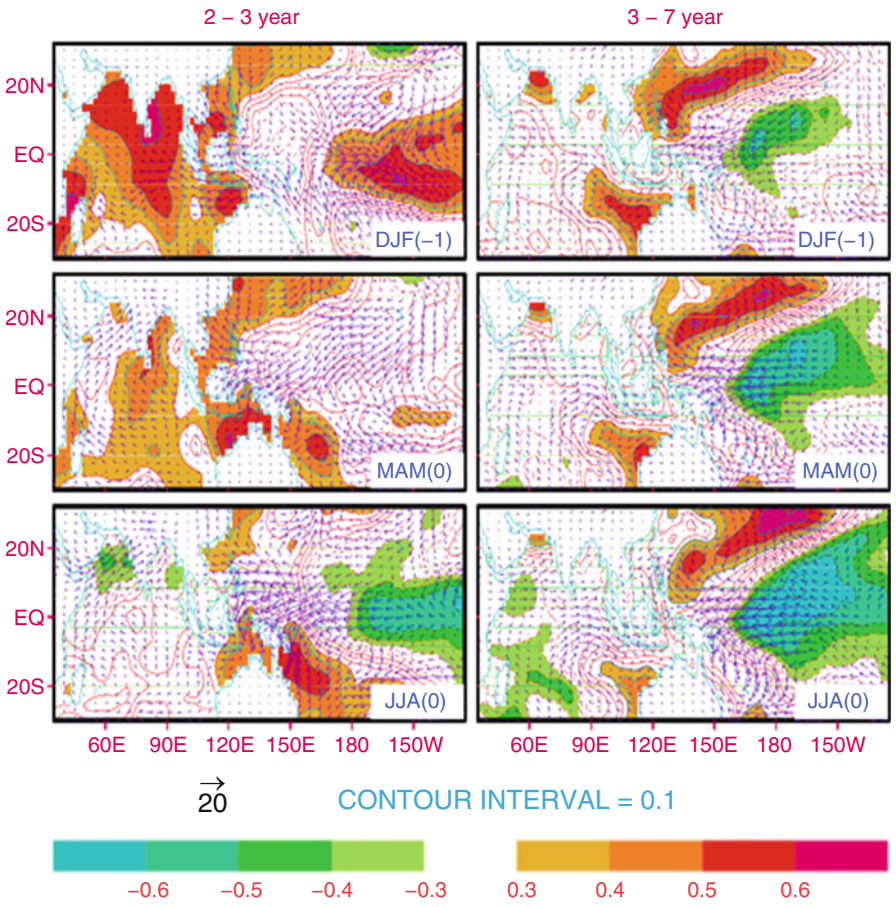

Fig. 6.10 Lagged correlation of the SSTA (*shading*) and lagged regression of 850-hPa wind with the all-Indian monsoon rainfall from the preceding winter to the concurrent summer for the 2–3-year (*left panel*) and 3–7-year (*right panel*) bands. The correlation above 0.4 corresponds to the 95% significance level or above (From Li et al. (2001). © Copyright 2001, American Geophysical Union (AGU))

of about 0.4 when taking into account the decrease of degrees of freedom due to the time filtering.) The fact that a warm IO SSTA leads to a wet monsoon implies that the IO SSTA may play an active role in affecting the Indian monsoon.

A warm SSTA in the IO in the preceding winter may result from the decrease of the prevailing northerly associated with a weak Asian winter monsoon. It is seen from Fig. 6.10 that the meridional wind at the surface is positively, lagged correlated (with a maximum correlation coefficient greater than 0.4) with the summer monsoon. This implies that a southerly wind anomaly appears over the northern IO in the preceding winter. The southerly wind anomaly can contribute to the ocean warming through (1) reduced surface evaporation (because the mean wind is

northerly in northern winter) and (2) anomalous meridional temperature advection that brings warmer water from the south. Thus, on the TBO timescale, a strong Indian summer monsoon is preceded by a weak winter Asian monsoon that is characterized by anomalous southerly over the northern IO.

Another notable feature associated with the monsoon TBO mode is the phase reversal of the EP SSTA in spring. The SST correlation coefficient changes its sign from a positive value in the preceding winter to a negative value in summer. Associated with this SSTA phase transition, the surface wind anomaly switches from westerly to easterly in the central equatorial Pacific.

In contrast to their high lagged correlation, the simultaneous correlation between the Indian monsoon and the IO SSTA is very low. This is because a strong Indian monsoon generates strong surface winds that further cool the ocean through enhanced surface evaporation and ocean mixing. As a result, the SSTA weakens rapidly in summer in the northern IO, especially along the eastern coast of Africa and in the Arabian Sea.

For the monsoon LF mode, the most significant SST correlation appears in the Pacific. While the WP SSTA has a positive, lagged correlation (+0.4) with the monsoon in the preceding winter, the EP SSTA has a simultaneous negative correlation (−0.5). The correlation with the IO SSTA is weak for all seasons prior to the monsoon onset, whereas a negative correlation appears after the monsoon onset, indicating a strong monsoon impact on the IO SSTA.

A common feature in both the 2–3-year and 3–7-year bands is that there is a strong simultaneous, negative correlation between the Indian monsoon and the EP SSTA. This points out an interactive nature of the monsoon–ENSO system. On one hand, a positive (negative) SSTA may have a remote impact on the monsoon through large-scale vertical overturning (Meehl 1987). On the other hand, anomalous monsoon heating may alter the EP SST through the change of winds over the central and western Pacific (Chang and Li 2001).

To examine the effect of anomalous moisture transport, we composite the 1000 hPa moisture flux convergence field based on the NCEP/NCAR reanalysis data. Ten wettest and ten driest years are selected based on the filtered monsoon rainfall data for both bands. From wet-minus-dry composites, one can see that in the 2–3-year band, there is significant low-level moisture convergence over the Indian subcontinent in the preceding winter and spring. In the 3–7-year band, the anomalous moisture flux convergence is quite different – no significant moisture convergence appears in the Indian subcontinent.

The Walker circulation is regarded as an important agent that links the Pacific Ocean to the Asian monsoon. Since the vertical motion in the mid-troposphere is related to upper and lower tropospheric divergent flows, we use the velocity potential difference (VPD) between 850 and 200 hPa to represent the vertical overturning cell of the Walker circulation. A positive (negative) VPD center corresponds to a strong ascending (descending) motion. Figure 6.11 illustrates the composite VPD field for the 3–7 year bands. A similar feature in both bands is that in summer (JJA), the Walker circulation is characterized by a strong ascending (descending) branch over the monsoon (EP) region. However, the evolution of the

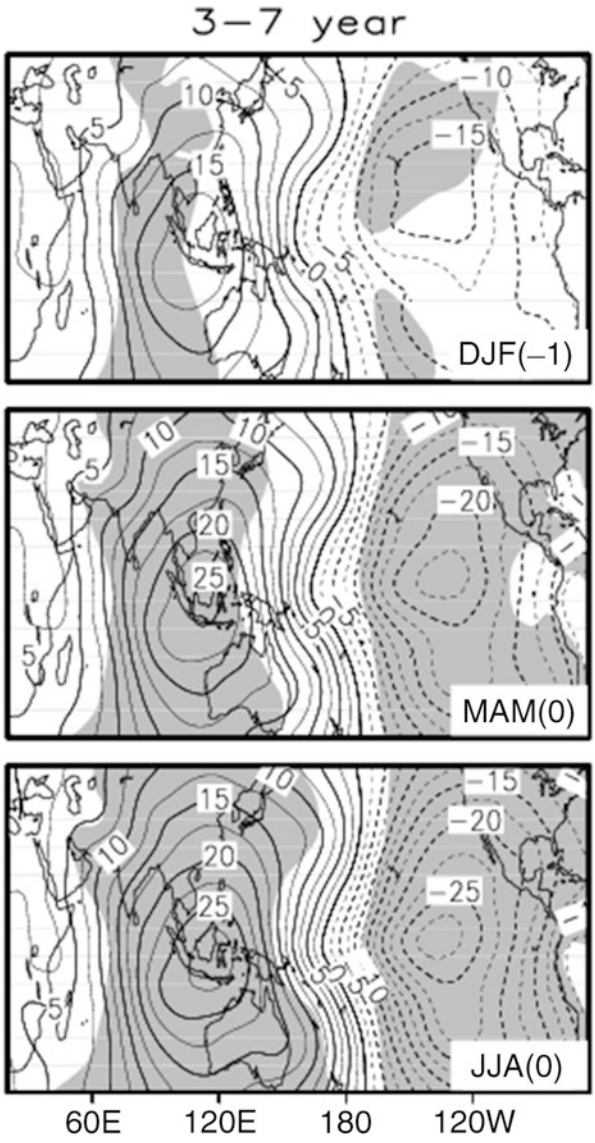

Fig. 6.11 Wet-minus-dry composites of the velocity potential difference (850 hPa minus 200 hPa) field in DJF (−1), MAM (0), and JJA (0) for the 3–7-year bands. The shaded regions represent the statistical significance of 95% and above

Walker cell in the two bands is quite different. For the LF mode, the ascending and descending branches are almost stationary, whereas for the QB mode, there is slow eastward propagation of the ascending and descending branches. This temporal evolution feature is somewhat similar to that found by Barnett (1991). Another feature in the 2–3 year band is that even though there is a remote SSTA forcing in the EP in winter, an ascending branch appears in the equatorial IO. This ascending motion results from the direct impact of the warm SSTA in the IO, which

compensates the effect of the El Niño in the EP. Thus, in addition to its moisture effect, the IO SSTA may have a dynamic impact on the vertical overturning of the Walker cell.

The land–ocean thermal contrast between the Asian continent and Indian Ocean was regarded as a good indication of the monsoon strength (e.g., Li and Yanai 1996; Yang et al. 1996). To examine the role of the land–ocean thermal contrast on the monsoon variability, we calculated the lagged correlation between the monsoon rainfall and the mean (between 200 and 500 hPa) tropospheric temperature. Figure 6.12 shows the lagged correlation maps. At the 2–3-year window (left panel), the increase of the tropospheric mean temperature is concurrent with the warming of the SST in the IO in the preceding winter and spring, while no significant temperature changes are found over the Eurasian continent. At the 3–7-year window (right panel of Fig. 6.12), a significant warming of the tropospheric mean temperature appears over the subtropical Eurasian continent in the preceding winter, with the correlation coefficient greater than 0.7. Meanwhile, a negative correlation center is located over the western equatorial IO. This north–south thermal contrast is even enhanced in northern spring and is significantly correlated with the summer monsoon rainfall. The physical processes that give rise to such a land–ocean thermal contrast are not clear, although several investigators (e.g., Meehl 1997; Yang and Lau 1998) have hypothesized that it might result from remote SST forcing in the tropics. The establishment of the meridional temperature gradient in the preceding season may help to set up the monsoon southwesterly earlier and stronger.

The time-filtering analysis above shows that the monsoon QB and LF modes have distinctive spatial and temporal structures. For the QB mode, a positive SSTA in the IO leads to a wet monsoon and the SSTA in the EP changes its phase in spring, whereas for the LF mode, a cold SSTA in the EP persists from winter to summer and is associated with a wet monsoon.

The time-filtering analysis indicates that the Indian monsoon rainfall is significantly correlated with the IO SSTA in the preceding winter and spring on the TBO timescale. A natural question is through what process the IO SSTA in the preceding seasons influences the monsoon. The IO SSTA may influence the Indian monsoon via both dynamic and thermodynamic effects. The dynamic impact is through induced upward motion in the monsoon sector that may compensate the effect of El Niño forcing from the EP. The thermodynamic impact is through the moisture effect. We argue that a warm SSTA can increase local moisture over the ocean through enhanced surface evaporation. The overall increase of specific humidity over the Indian Ocean is a good precondition for a strong monsoon, because after the monsoon onset, the southwesterly flows would transport these excess moistures into the monsoon region. A strong monsoon enhances surface winds that cool the ocean through surface evaporation and ocean mixing, resulting in a colder than normal IO SSTA that further reduces the moisture accumulation and leads to a weak monsoon next year.

In addition to the IO SST, the low-level moisture convergence in the preceding spring is significantly correlated with the monsoon on the TBO timescale. We argue

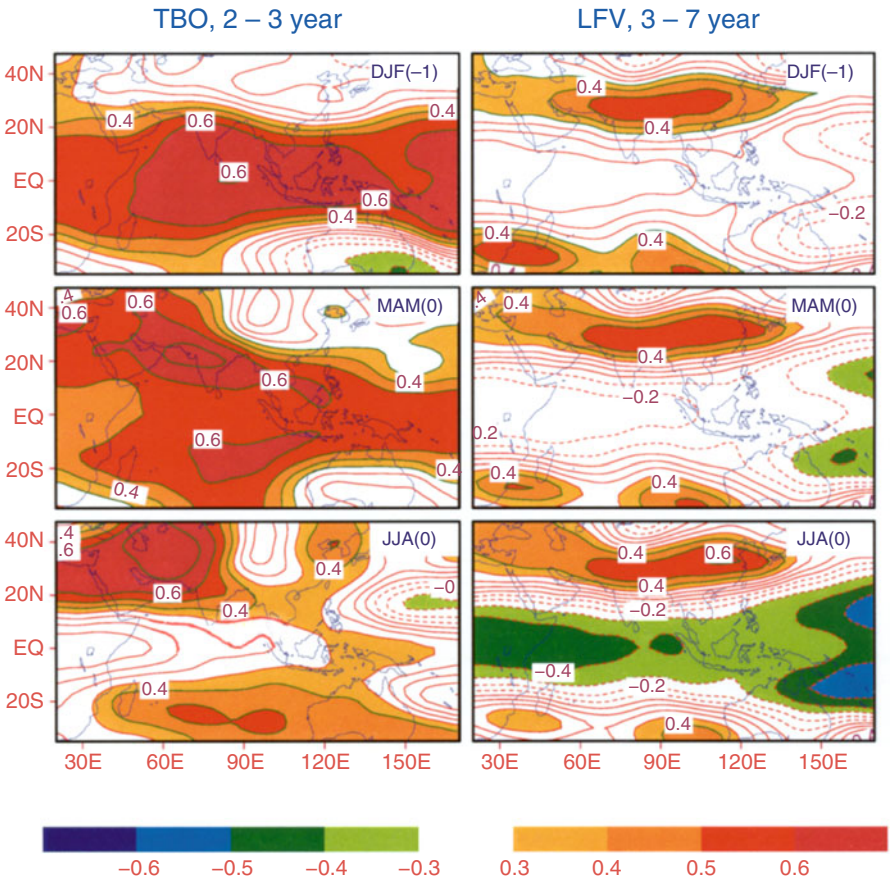

Fig. 6.12 Lagged correlation maps between the all-Indian monsoon rainfall and the mean tropospheric (200–500 hPa) temperature in DJF(−1), MAM(0), and JJA(0) for the 2–3-year and 3–7-year bands (contour interval, 0.1). The regions where the positive (negative) correlation exceeds 0.3 are heavily (lightly) shaded. The statistical significance exceeds the 95% level when the correlation is above 0.4 (From Li et al. (2001). © Copyright 2001, American Geophysical Union (AGU))

that the anomalous moisture convergence may influence the monsoon through the accumulation of local moisture. As we know, during the dry seasons, the local atmosphere over India is in a convectively stable regime. Because of that, the convergent water vapor prior to the monsoon onset can be used only for moistening the local air. The increase of local humidity may initially help strengthen the monsoon intensity, which may further induce anomalous southwesterly flows during the monsoon season and help to bring more moistures from the tropical ocean. Note that this anomalous moisture convergence mechanism differs from the effect of the IO SSTA. The former is associated with the moisture flux by

anomalous winds, whereas the latter is related to anomalous moisture advection by the mean monsoon flow.

While the monsoon TBO is primarily controlled by local processes, the monsoon LF variability might be due to the remote forcing of the SSTA in the Pacific. We argue that three possible processes may contribute to the rainfall anomaly on the lower-frequency timescale. The first is the direct impact of the EP SSTA through the vertical overturning of the large-scale east–west circulation (e.g., Meehl 1987). This mechanism can be readily seen from the wet-minus-dry composites of the velocity potential difference field (Fig. 6.11). The second is the effect of the anomalous SST in the WP. Associated with a cold SSTA in the equatorial EP, a positive SSTA appears in the WP. This warm SSTA may further affect local convective activity and induce anomalous lower tropospheric circulation off the Philippines (Tomita and Yasunari 1993). It is speculated that the enhanced convective activity in the WP may increase the frequency or intensity of the northwestward-propagating synoptic-scale disturbances and thus enhances the monsoon trough from the equatorial WP to the Indian subcontinent. The third process is attributed to the impact of the remote tropical SSTA forcing on the mid-latitude atmospheric circulation. The wet-minus-dry mean tropospheric temperature composite shows that 3–6 months prior to a wet monsoon, a north–south thermal contrast has already been established across South Asia and the IO, with the warm core centered over the Tibetan Plateau. The location of this warm core is consistent with the hypotheses that Tibetan heating and/or Eurasian snow cover prior to the monsoon onset play an important role in the strength of the monsoon (e.g., Mooley and Shukla 1987; Yanai et al. 1992). This differs markedly from the monsoon TBO mode, in which the Indian subcontinent and the IO are both covered by an elongated warm anomaly belt in the preceding winter and spring. Thus, an enhanced (reduced) land–ocean thermal contrast precedes a strong (weak) monsoon on the lower-frequency timescale but not on the TBO timescale.

6.4 Pacific–East Asia Teleconnection

Observational analyses indicate that while IM is primarily influenced by ENSO during its developing phase, the interannual variability of EAM is highly correlated with ENSO during its decaying phase. In the summer after an El Niño, the Meiyu/Baiu rainfall tends to be abundant (Huang and Wu 1989, Wang and Li 1990, Zhang et al. 1996; Lau and Yang 1996; Soman and Slingo 1997; Kawamura 1998), even though during that season, SST in the eastern equatorial Pacific is nearly normal (Fig. 6.13). Why does the ENSO have a delayed impact on the EAM?

To address this question, one must first reveal dominant seasonal evolving circulation patterns in the monsoon sector in association with the developing and decaying phases of ENSO. A season-sequence singular vector decomposition (SS-SVD) analysis method is applied, following Wang et al. (2003a, b). Figure 6.14 displays the evolution of anomalous 850 hPa winds and vertical p-velocity

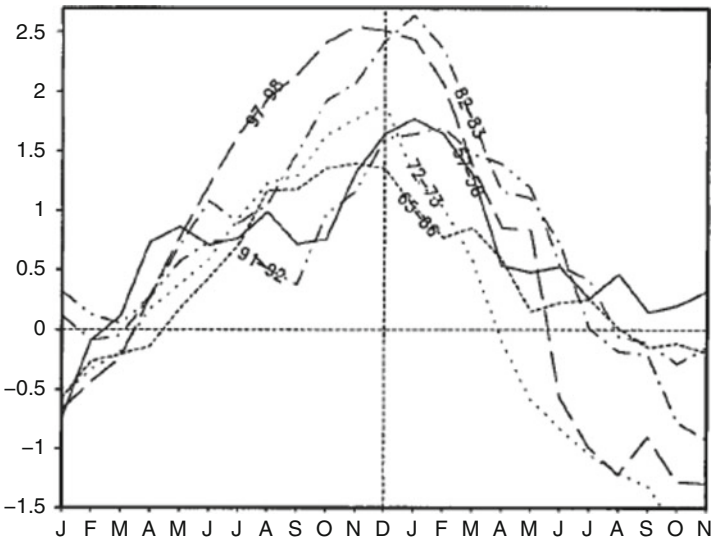

Fig. 6.13 Time evolution of Niño 3.4 SSTA for individual El Niño events during 1956–2000 (From Wang et al. (2000). © Copyright 2000 American Meteorological Society (AMS))

associated with ENSO turnabout revealed by the first SS-SVD mode. This mode describes 91% of the total covariance between the SST anomalies in the tropical Pacific and Indian Oceans (40°E–90°W, 20°S–20°N) and five seasonal mean 850 hPa wind anomalies.

During the summer when the El Niño develops, the low-level circulation anomalies are dominated by an elongated anticyclonic ridge extending from the Maritime Continent to the southern tip of the India. Associated with this anticyclonic ridge is a tilted belt of pronounced anomalous westerlies extending from the Bay of Bengal to the WNP, suppressed convection over the Maritime Continent, and enhanced convection over the Philippine Sea (Fig. 6.14a). The enhanced WNP monsoon trough greatly increases the number of tropical storm formation in the southeast quadrant of the tropical WNP (5°–17°N, 140°–170°E) (Chen et al. 1998; Wang and Chan 2002). On the other hand, the weak anticyclonic anomalies over India imply a moderately deficient ISM.

During the fall of El Niño developing year, the southern Indian Ocean (SIO) anticyclone grows explosively, leading to a giant anticyclonic ridge dominating the Indian Ocean with the anticyclone center at 10°S, 90°E, a tilted ridge extending from western Australia all the way to the Arabian Sea (Fig. 6.14b). Note that a new anomalous low-level anticyclone starts to form in the vicinity of Philippines.

In the mature phase of El Niño, D(0)/JF(1), the low-level circulation anomalies are dominated by two subtropical anticyclonic systems located in the SIO and the WNP, respectively (Fig. 6.14c). The former is a result of the weakening and eastward retreat of the SIO anticyclone from boreal fall, while the latter results

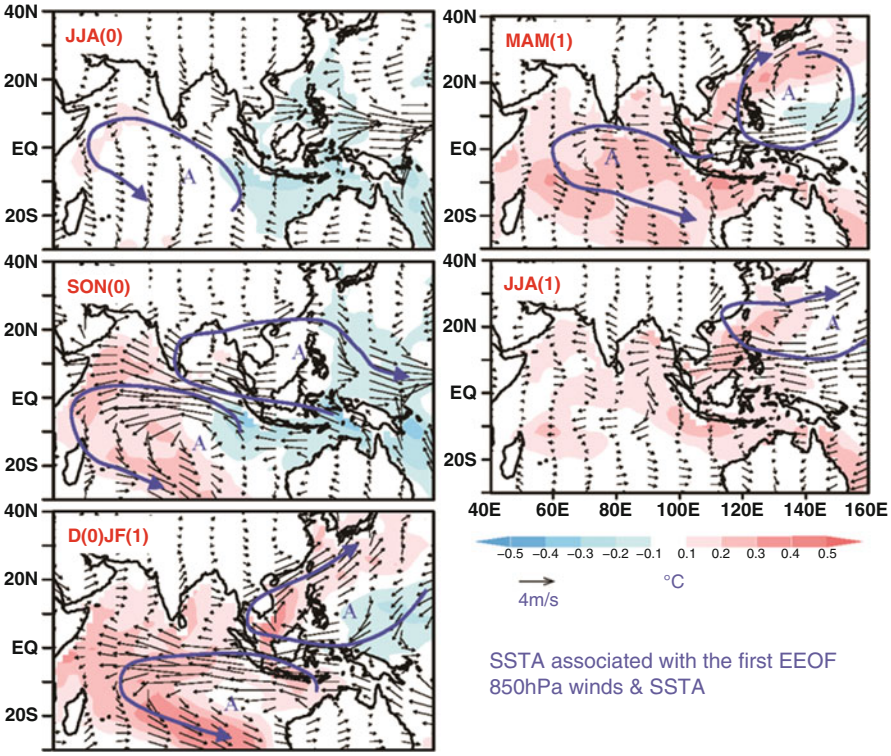

Fig. 6.14 Seasonal evolving patterns of 850-hPa wind (vector) and SST (*shading*) anomalies associated with El Niño turnabout from the developing summer, JJA(0), to the decaying summer, JJA(1), calculated based on the SS-SVD analysis (From Wang et al. (2003b). © Copyright 2003 American Meteorological Society (AMS))

from the amplification and eastward migration of the Philippine anticyclone. The most suppressed convection centered east of Philippine.

MAM(1) and JJA(1) have similar anomaly patterns, which are characterized by the pronounced WNP anomalous anticyclone (Fig. 6.14d and e). The intensity of the WNP anticyclone, however, decreases toward JJA(1). By summer JJA(1), subsidence controls the Philippine Sea and Southeast Asia, signifying weakening of the summer monsoon over the WNP and South Asia. The anomaly pattern exhibits nearly opposing polarities with that in the summer of the previous year, indicating a strong biennial tendency associated with the El Niño turnabout.

The most interesting feature of the seasonal evolving monsoon patterns in Fig. 6.14 is the persistence of the anomalous anticyclone in WNP from the El Niño peak winter to the subsequent summer. It is the anomalous anticyclone in JJA (1) that leads to enhanced rainfall in the Meiyu region through enhanced pressure gradients and moisture transport (Chang et al. 2000a, b). As the atmosphere itself does not hold a long memory, the persistence of the anomalous Philippine Sea

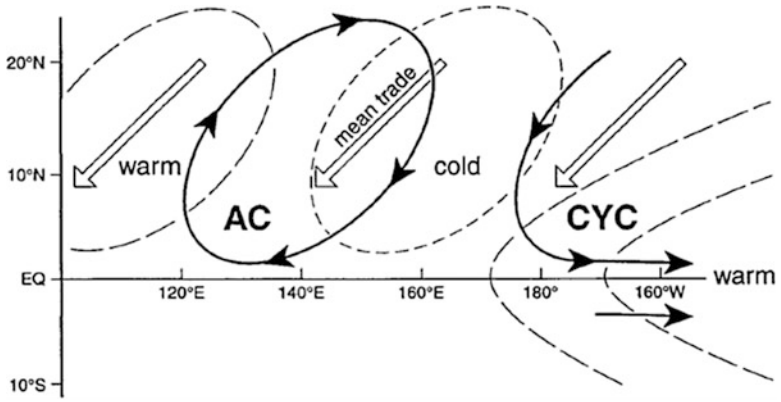

Fig. 6.15 A schematic diagram illustrating the effect of a positive air–sea feedback between the PSAC and cold SSTA in WNP. The *double arrow* denotes the background mean trade wind, and heavy lines with *black arrows* represent the anomalous wind. The long (short) *dashed lines* represent a positive (negative) SSTA (From Wang et al. (2000). © Copyright 2000 American Meteorological Society (AMS))

anticyclone (PSAC) from the boreal winter to summer calls for a dynamic explanation.

The process through which ENSO has a delayed impact on the EAM was illustrated by Wang et al. (2000) (see a schematic diagram in Fig. 6.15). The essential part of the proposed mechanism lies in a local positive air–sea feedback between atmospheric descending Rossby waves and the underlying cold SST anomaly in WNP that maintains the anomalous PSAC from the mature El Niño to the ensuing summer. This positive feedback, operated in the presence of background northeasterly trade winds, may be described as follows: to the east of the anomalous PSAC, the increased total wind speed cools the ocean surface where it induces excessive evaporation and entrainment. The cooling, in turn, suppresses convection and reduces latent heating in the atmosphere, which excites descending atmospheric Rossby waves that reinforce the PSAC in their decaying journey to the west. The initial triggering of the cold SSTA may be attributed to the atmospheric Rossby wave responses to the central equatorial Pacific heating during the El Niño peak winter – the so-induced anomalous flows coincide with the background mean wind and lead to enhanced evaporation and thus the cooling of the local ocean surface. The initial triggering of an anomalous PSAC may arise from the cold surge intrusion from the Asian continent (Wang and Zhang 2002) or the eastward propagation of a low-level anticyclone from the tropical Indian Ocean (Chen et al. 2007).

In contrast to its weakening in the El Niño decaying summer, the WNPM tends to strengthen in the El Niño developing summer (Fig. 6.14). The possible cause of this enhancement during the El Niño developing phase is as follows: First, it is attributed to the increases of low-level cyclonic vorticity associated with equatorial westerly anomalies. Secondly, in response to El Niño forcing, convection over the

Maritime Continent is suppressed. The suppressed convection leads to an equatorial-asymmetric atmospheric Rossby wave response in the presence of the asymmetry of easterly shear of the summer mean zonal flow (Wang et al. 2003b). Thus, a strong anticyclonic cell appears north of the equator, with an anomalous ridge tilted northwestward toward the Indian subcontinent. This leads dry monsoon over India. Meanwhile, the anomalous anticyclonic flow enhances low-level westerlies and thus convective activities over the WNP. This explains the observed negative correlation between the interannual anomalies of the IM and WNPM.

6.5 Effects of Indian Ocean and WNP SSTA on Circulation in WNP

6.5.1 Season-Dependent Indian Ocean SSTA Forcing Effect

Figure 6.16 shows the composite anomalous atmospheric circulation and SST fields associated with El Niño composite from El Niño mature winter (DJF) to the subsequent summer (JJA) during 1950–2006. Note that an anomalous anticyclone persists in the tropical WNP from El Niño mature winter to the subsequent summer. It is this anomalous anticyclone that causes devastating rainfall in central China during the El Niño decaying summer.

What maintains the anomalous anticyclone from the winter to summer? The positive thermodynamic air–sea interaction mechanism illustrated by Fig. 6.15 may

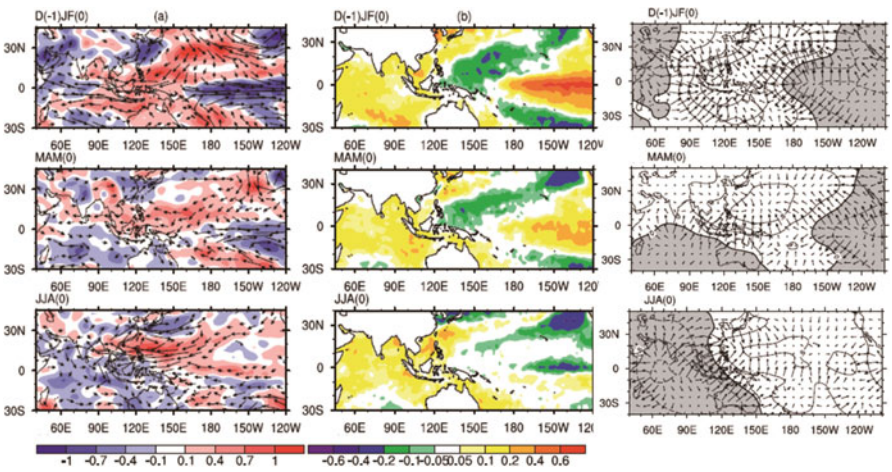

Fig. 6.16 Seasonal evolution patterns of (*left*) anomalous 850 hPa wind (vector) and 500 hPa vertical p-velocity, (*middle*) SST and (*right*) 200 hPa velocity potential fields derived from 12 El Niño composite from El Niño mature winter to the subsequent summer during 1950–2006 (From Wu et al. (2009). © Copyright 2009 American Meteorological Society (AMS))

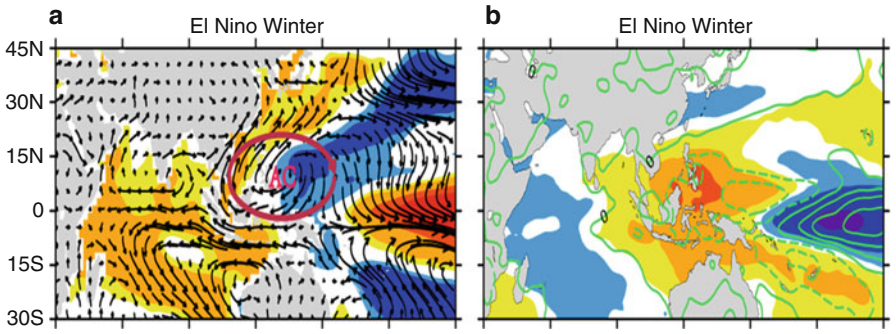

Fig. 6.17 Composite patterns of 925 hPa wind (vectors; unit, m/s) and SSTA (*shading*; unit, °C) fields (*left*) and OLR (*shading*; unit, W/m^2) and precipitation (contours; unit, mm) fields (*right*) during El Niño mature phase (DJF). Composite is based on 1980–2013 (From Chen et al. (2016). © Copyright 2016 American Meteorological Society (AMS))

explain its maintenance from northern winter to spring, as the mean flow is northeasterly during this period, but in the summer after the mean flow switches its direction, it becomes a negative feedback. Meanwhile, in association with El Niño decaying, an Indian Ocean basin-wide warming is observed, and this basin-wide warming persists from El Niño mature winter to the subsequent summer. Does the Indian Ocean SSTA play a role in affecting WNP anomalous circulation?

A study by Wu et al. (2009) argued that the Indian Ocean basin-wide warming can only have an impact on the WNP anomalous anticyclone in El Niño decaying summer, not in El Niño mature winter and following spring. The following is the physical reasoning.

Although the basin-wide SSTA pattern occurs in IO, rainfall and OLR anomalies show a clear east–west dipole structure, with enhanced (suppressed) convection over the western (eastern) IO. Prior to this season, the SSTA in IO is dominated by a zonal dipole, with strong cooling in the eastern pole. The rapid warming in eastern IO from northern fall to winter is attributed to both strengthened shortwave radiation forcing and ocean wave effect (Li et al. 2003; Hong et al. 2010).

The observed IO rainfall–SST relationship (Fig. 6.17) in El Niño mature winter implies a distinctive role the SSTA plays in affecting local convection and circulation. While the local warming in the eastern IO plays a passive role (i.e., it is local atmosphere that influences the ocean), the SSTA in the western IO plays an active role in strengthening atmospheric convection (i.e., it is the ocean that primarily influences the atmosphere) (Wu et al. 2009, 2012).

Given such a complex relationship, one needs to be cautious when designing numerical model experiments. Forced SSTA experiments may lead to a basin-wide precipitation anomaly over IO, which according to Gill's (1980) solution, would lead to a response of low-level easterlies in the western equatorial Pacific. Rainfall anomalies simulated by this forced experiment, however, were against the observed rainfall pattern.

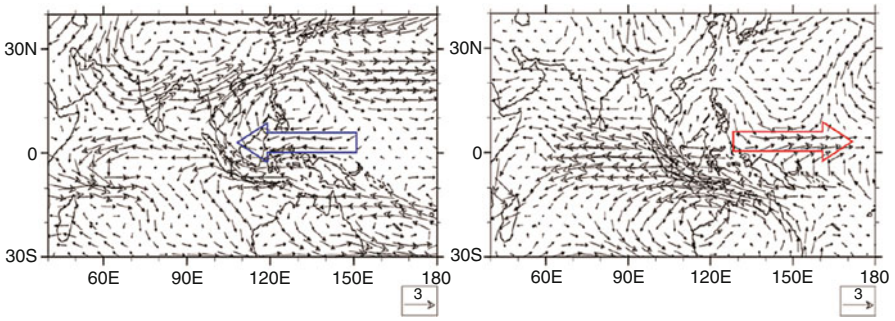

Fig. 6.18 The 850 hPa wind anomaly fields (vectors; unit, m/s) simulated from ECHAM4 in response to a specified SSTA forcing in tropical Indian Ocean (IO; *left*) and in response to a specified diabatic heating anomaly in the tropical IO (*right*). The *blue* vector denotes anomalous easterly wind, and red vector denotes anomalous westerly wind (From Chen et al. (2016). © Copyright 2016 American Meteorological Society (AMS))

To demonstrate how a specified SSTA experiment in IO might "screw up" the atmospheric response in WP, we conducted a control experiment (in which the climatologic monthly SST is specified everywhere in the ocean) and two sensitivity experiments using ECHAM4. In the first sensitivity experiment, the observed SSTA in IO (same as that shown in Fig. 6.17a) is superposed onto the climatologic SST field. In the second sensitivity experiment, a dipole heating pattern that has the same horizontal pattern as the precipitation anomaly shown in Fig. 6.17b and an idealized vertical profile that has a maximum at middle troposphere is specified. Figure 6.18 shows the model simulation result from the two experiments. As expected, a basin-wide precipitation anomaly occurs in the specified SSTA experiment; as a result the low-level wind anomaly in equatorial WP is dominated by easterlies. In contrast, a westerly anomaly appears in the equatorial WP in the specified heating experiment because anomalous descending (ascending) motion in eastern (western) IO favors a reversed Walker circulation in both the tropical IO and Pacific.

The numerical experiments above indicate that a caution is needed in designing idealized atmospheric model experiments with specified SSTA forcing. It is important to compare observed and simulated rainfall anomalies in the specified SSTA region, to make sure that the local heating anomaly pattern is realistic.

While the anomalous vertical motion or precipitation field in the IO has a dominant east–west dipole pattern in El Niño mature winter, it becomes a north–south dipole in the subsequent spring, with anomalous ascending motion south of the equator (Fig. 6.16). Only in the summer following a peak El Niño, when SSTA in the eastern equatorial Pacific has dissipated, a basin-wide anomalous ascending motion and precipitation was observed. Such a basin-wide feature was also seen in the 200 hPa velocity potential field (Fig. 6.16). This points out that only in this season the basin-wide SSTA in IO can induce a basin-wide large-scale convective heating, which can further impact the circulation remotely in the Pacific.

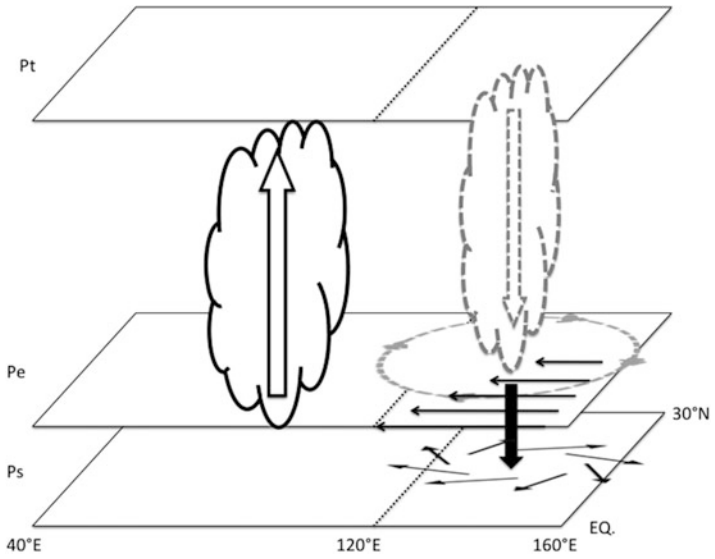

Fig. 6.19 Schematic diagram illustrating the impact of IO basin-wide heating on WNP anomalous anticyclone during El Niño decaying summer (From Wu et al. (2009). © Copyright 2009 American Meteorological Society (AMS))

Schematic diagram Fig. 6.19 describes how the basin-wide convection in IO can impact the anomalous anticyclone in the WNP. In response to basin-wide equatorial convective heating in IO, a Kelvin wave response with easterly anomalies appears in the western Pacific (Gill 1982). This Kelvin wave response has maximum amplitude at the equator, decreasing with increased latitudes. Anomalous anticyclonic shear north of the equator associated with this Kelvin wave response causes anomalous divergence and descending motion in the PBL, leading to the reduction of PBL specific humidity. The reduced moisture suppresses the monsoon heating, which can further induce low-level anomalous anticyclone in the WNP. Through this remote forcing mechanism, IO impacts the WNP circulation during El Niño decaying summer. This mechanism was called as IO capacity effect by Xie et al. (2009).

6.5.2 Relative Role of Indian Ocean and WNP SSTA Forcing

As discussed in the previous section, the maintenance of the WNPAC from the El Niño mature winter to the subsequent spring is attributed to a positive thermodynamic air–sea feedback. A cold SSTA in the WNP suppresses local convection, which stimulates low-level atmospheric anticyclone anomaly to its west. The northeasterly anomalies to the eastern flank of the WNPAC enhance the mean

trade wind and cool the SST in situ through enhanced surface latent heat flux (Wang et al. 2000).

With the onset of the WNP summer monsoon, the mean southwesterly monsoon circulation replaces the northeasterly trade wind. As a result, a negative evaporation–wind–SST feedback appears in the region. The negative air–sea feedback weakens the negative SSTA in the WNP throughout the El Niño decaying summer. In contrast to the weakening of the local negative SSTA, the WNPAC is strengthened from the preceding spring to the summer (Fig. 6.16).

A possible cause of strengthening of the WNPAC during the El Niño decaying summer is attributed to the remote SSTA forcing from the tropical Indian Ocean (TIO) (Wu et al. 2009; Xie et al. 2009). An Indian Ocean basin mode (IOBM) establishes after the ENSO mature winter. The basin-wide warming in the TIO is possibly caused by anomalous surface heat flux associated with the descending branch of the anomalous Walker circulation (Klein et al. 1999; Lau and Nath 2003) or the change of tropical tropospheric temperature (Chiang and Sobel 2002). In addition, ocean dynamic processes also play a role (Li et al. 2003). The IOBM may strengthen the WNPAC in boreal summer through the following two processes. Firstly, through enhanced convection over the TIO, the IOBM may stimulate a Kelvin wave-type easterly response in the western Pacific. The anticyclonic shear vorticity associated with the easterly anomalies may weaken the WNP summer monsoon through Ekman pumping divergences (Wu et al. 2009). Secondly, the IOBM may increase the surface moisture and thus enhance the low-level moisture transport and convection over the Maritime Continent, the latter of which may further induce the subsidence over the WNP through anomalous Hadley circulation (Chang and Li 2000; Li et al. 2001; Sui et al. 2007).

It appears that both the local forcing of the negative SSTA in the WNP and the remote SSTA forcing from the TIO may impact the WNPAC during the El Niño decaying summer. However, their relative contributions are still not clear.

Idealized numerical model experiments were designed to reveal the relative contribution from the TIO and western Pacific (WP) SSTA forcing. In a control run (CTRL), ECHAM4 was integrated for 20 years, forced by monthly climatological SST. In three sets of sensitivity experiments, the composite SSTA pattern in the global ocean (hereafter GB run), the TIO only (hereafter IND run), or the WP only (hereafter WP run) was added to the climatological SST as the model's lower boundary condition. Note that in the IND (WP) run, the SST climatology was prescribed in the regions outside of the TIO (WP). Each experiment was integrated from April to August, with 20 ensemble members. The ensemble mean results of June, July, and August are analyzed.

The difference between the GB and CTRL runs provides an evaluation on the performance of the model in reproducing the WNPAC. The difference between the IND and CTRL runs examines the sole contribution of the remote IOBM forcing to the WNPAC, and the difference between the WP and CTRL runs examines the sole contribution of the local WP SSTA forcing.

The above numerical sensitivity experiments demonstrate that both the remote IOBM forcing and the local WP SSTA forcing contribute to the maintenance of the

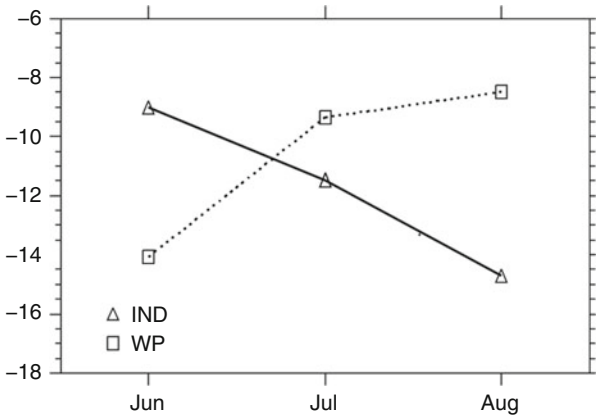

Fig. 6.20 Temporal evolutions of area-averaged vorticity anomalies (units, 10^{-6} m^2 s^{-1}) over the region of 10–35°N, 115–160°E for the WP (*dashed line*) and IND (*solid lines*) runs (From Wu et al. (2010). © Copyright 2010 American Meteorological Society (AMS))

WNPAC during the El Niño decaying summer. Figure 6.20 shows area-averaged vorticity anomaly over the WNP region (10°–35°N, 115°–160°E) from June to August derived from the WP and IND runs. The amplitude of JJA mean vorticity anomalies from the two runs are comparable, indicating that both the local WP SSTA forcing and remote TIO SSTA forcing are equally important in maintaining the WNPAC during El Niño decaying summer. A further examination of sub-seasonal evolutions of the two runs reveals an interesting difference. The local WP SSTA forcing leads to the strongest WNPAC response in June, and such a response weakens quickly in July and August. The remote TIO forcing, on the other hand, is relatively weak in early summer and strengthens greatly toward the end of the summer. What causes such a difference?

In the WP run, the WNPAC is primarily forced by the local negative SSTA. A significant large negative SSTA appears in the WNP prior to the El Niño decaying summer due to a positive thermodynamic air–sea feedback, as discussed in the previous section. As the summer comes, the reversal of the mean wind leads to a negative air–sea feedback. Despite of this negative feedback, the cold SSTA in the WNP is still quite large in June and July (Fig. 6.16) and affecting the local circulation anomaly in situ. The decay of the local SSTA forcing due to a negative feedback leads to the continuous weakening of the simulated WNPAC from June to August.

Different from the WP run, the evolution of the WNPAC in the IND run is associated with the sub-seasonal change of the background mean flow. The WNP monsoon trough becomes fully developed only in the later summer (after July 15). Although the amplitude of the IOBM weakens slightly from June to August, the simulated WNPAC intensifies with time and expands eastward. The intensification and expansion are consistent with the establishment of the climatological WNP monsoon trough in late summer. As a Kelvin wave response to positive heating anomalies in the tropical Indian Ocean, easterly anomalies in the western Pacific cause an anticyclonic shear and thus a boundary layer divergence over the WNP through Ekman pumping (Wu et al. 2009). The boundary layer divergence leads to

a greater negative precipitation anomaly response in late summer, when the monsoon trough is fully established. This explains why the remote Indian Ocean forcing effect is strengthened from June to August even though the IOBM weakens.

In summary, the WNPAC during the El Niño decaying summer is attributed to both the remote TIO and local WNP SSTA forcing. In early summer, the WNPAC is primarily influenced by the local negative SSTA, whereas in late summer, the IOBM plays a more important role in maintaining the WNPAC.

6.6 Modulation of the Monsoon Mean Flow on El Niño Response

Figure 6.21 shows the pattern of composite precipitation and low-level circulation anomalies during El Niño developing summer. Note that during the El Niño forcing, large-scale negative rainfall anomalies appear over the Maritime Continent. Two Rossby wave gyres occur to the west of the large-scale negative heating anomaly over the Maritime Continent. It is interesting to note that the two gyres, one at south of the equator and another at north of the equator, are not symmetric about the equator. The northern gyre is much greater.

Why is the circulation response asymmetric to a symmetric El Niño forcing? It is hypothesized that the asymmetric response is primarily attributed to the equatorial asymmetry of the summer mean flow, in particular the mean vertical shear. Figure 6.22a shows that background vertical shear in boreal summer is asymmetric about the equator. Over the Indian monsoon region, there are pronounced low-level westerlies and upper-level easterlies. As a result, there is strong background

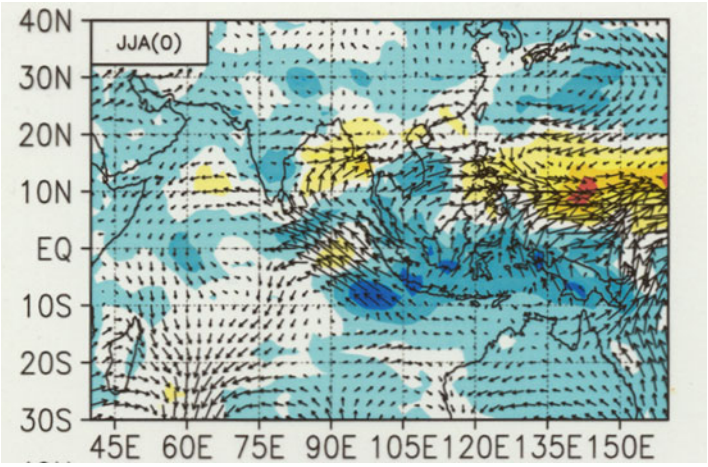

Fig. 6.21 Pattern of composite precipitation and 925 hPa wind anomalies during El Niño developing summer. The composite is based on all El Niño cases during 1950–2006

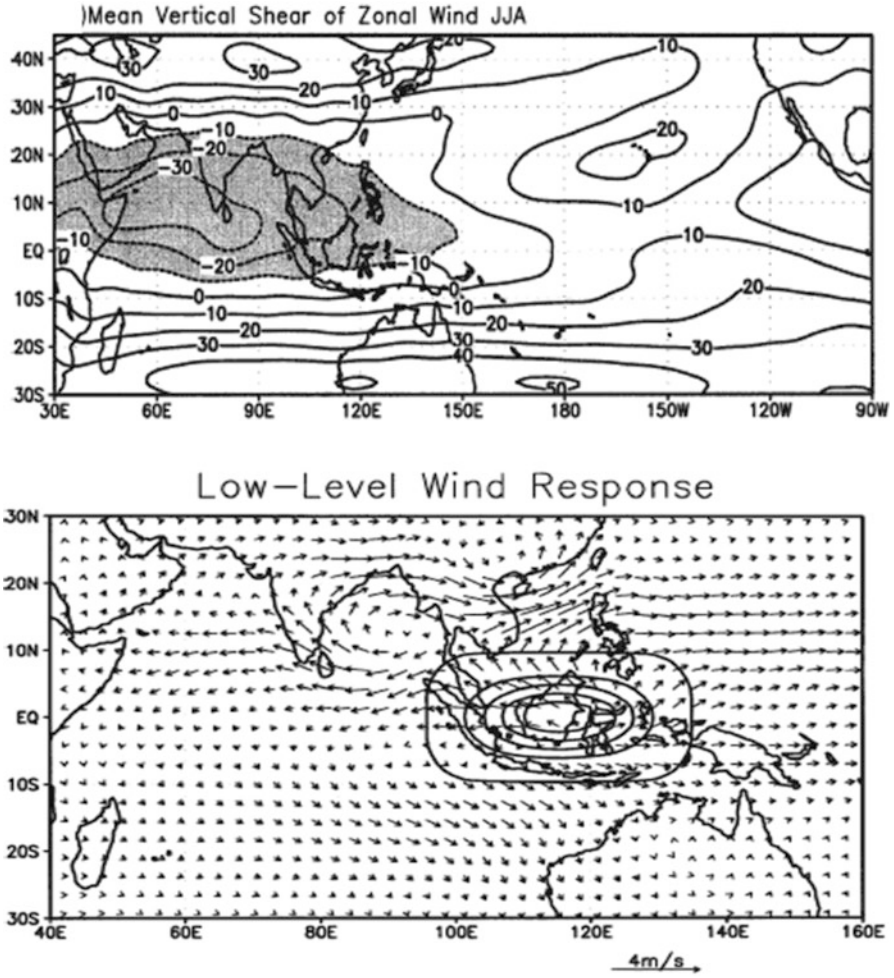

Fig. 6.22 (*Top*) The pattern of vertical shear of climatological zonal wind between 200 and 850 hPa averaged in JJA. (*Bottom*) Low-level wind response to a specified negative heating anomaly over the Maritime Continent simulated by an anomalous AGCM in which observed summer mean flow is specified as a background state (From Wang et al. (2003a, b). © Copyright 2003 American Meteorological Society (AMS))

easterly vertical shear in the northern Indian Ocean, while the shear is much weaker in the southern Indian Ocean. A theoretical study by Wang and Xie (1996) showed that background easterly (westerly) shear favors the growth of tropical Rossby wave type perturbations in the lower (upper) troposphere. Because energy source in the tropics is primarily latent heat, a stronger lower-tropospheric vorticity would favor a stronger PBL moisture convergence and a thus a stronger convective feedback (Li 2006).

To examine how the background mean flow modulates the anomalous circulation response in the Indo-western Pacific region, we conducted an anomaly GCM experiment, in which the summer mean flow is specified, and an equatorially symmetric negative heating anomaly is specified in the Maritime Continent (to mimic the direct El Niño forcing effect). The bottom in Fig. 6.22 illustrates the low-level circulation anomaly response to this prescribed symmetric heating. Similar to the observed, a greater Rossby wave gyre response appears in the northern hemisphere. Thus, the modeling study confirms the effect of the asymmetric summer mean flow in regulating the El Niño teleconnection pattern in South Asia/TIO.

6.7 Inter-monsoon Relationships

Meehl (1987) pointed out an in-phase relationship between the Indian summer monsoon (IM) and Australian summer monsoon (AM), based on limited data. Is this relationship steady? How is this relationship comparable to phase relations between WNP summer monsoon (WNPM) and IM/AM?

Gu et al. (2010) examined the relationship among three tropical monsoons, IM, WNPM, and AM, using different reanalysis datasets. Table 6.1 shows the correlations among the time series of the WNPM, AM, and IM intensity indices from 1979 to 2005. The correlation coefficient between WNPM and the preceding AM is 0.37, passing the 90% significance level. This implies that a strong (weak) AM might be associated with a succeeding strong (weak) WNPM. This in-phase relation appears in 19 out of the total 27 years. By checking winter (DJF) Niño3.4 index for each WNPM-AM in-phase years, we found that the eastern Pacific SSTA is all positive (negative) for the negative (positive) strong in-phase events, implying that ENSO is a major controlling factor for the AM-WNPM in-phase relationship.

The correlation coefficient between WNPM and the succeeding AM is −0.41, exceeding the 95% significance level. This points out an out-of-phase relation between the two sub-monsoon systems, that is, a strong (weak) WNPM often

Table 6.1 Lagged correlation coefficients among WNPM, IM, and AM for 1979–2005 using NCEP-DOE and CMAP

From	IM	AM	***WNPM***	***AM***	***WNPM***
	JJA(0)	DJF(0)	***JJA(0)***	***DJF(0)***	***JJA(0)***
To	AM	IM	***AM***	***WNPM***	***IM***
	DJF(1)	JJA(0)	***DJF(1)***	***JJA(0)***	***JJA(0)***
Correlation coefficient	0.29	−0.28	***−0.41***	***0.37***	***−0.64***
Number of events	17	17	***17***	***19***	***17***

From Gu et al. (2010). © Copyright 2010 American Meteorological Society (AMS)
Note: The 90% (95%) significance level corresponds to a correlation coefficient of 0.32 (0.38). Number of events indicates the number of years during which the relationship between two monsoons is consistent with the correlation coefficient

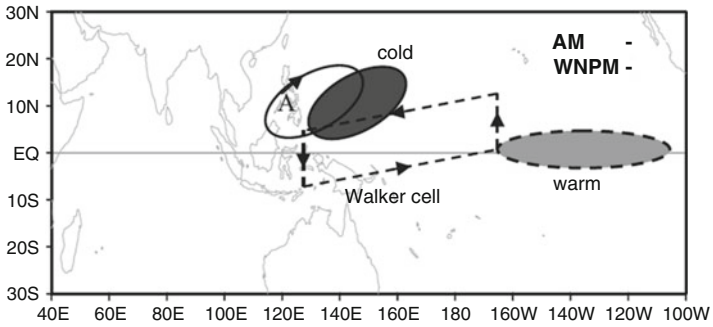

Fig. 6.23 Schematic diagram showing DJF (*dashed line*) and JJA (*solid line*) processes responsible for in-phase relation from AM to the succeeding WNPM (From Gu et al. (2010). © Copyright 2010 American Meteorological Society (AMS))

leads a weak (strong) AM. A further examination shows that about two thirds of all events reflect the out-of-phase relationship.

The most significant correlation appears in the simultaneous correlation between WNPM and IM, which is −0.64, passing the 99% significance level. This simultaneous out-of-phase relation appears in 17 summers during 1979–2005.

As seen from Table 6.1, compared with the correlations between the WNPM and AM/IM, the correlation coefficients between IM and AM are relatively weak and not statistically significant. Different from the many previous studies that made composites based on El Niño and La Niña conditions, the composite here is based on the anomalous monsoon intensity. In the following we will particularly focus on the phase relations of WNPM with other two sub-monsoon systems, as they are most significant relationships. The strategy is to examine the circulation and SST evolution characteristics to find the common features and similar physical mechanisms that control these relationships.

Figures 6.23, 6.24, and 6.25 are schematic diagrams illustrating the essential physical processes that may contribute to each of the sub-monsoon phase relations. The in-phase relationship from AM to the succeeding WNPM occurs primarily during the ENSO decaying phase (Fig. 6.23). On the one hand, the warm SSTA in the eastern Pacific induces a reversed anomalous Walker cell and causes a weak AM during the El Niño mature winter. On the other hand, an anomalous anticyclone is induced in WNP through either the Pacific–East Asia teleconnection (Wang et al. 2000; Wang and Zhang 2002) or the eastward propagation of a low-level anticyclone anomaly in the tropical Indian Ocean (Chen et al. 2007). The WNP anomalous anticyclone is maintained through a positive local thermodynamic air–sea feedback between the anticyclone and a cold SSTA (Wang et al. 2003a, b) from the boreal winter to late spring in the presence of the mean northeasterly. The local cold SSTA leads to a weak WNPM in boreal summer.

The out-of-phase relation from WNPM to the succeeding AM includes two different scenarios (Fig. 6.24). Scenario 1 describes the El Niño early onset or the La Niña persistence events. Scenario 2 consists of El Niño decaying/La Niña

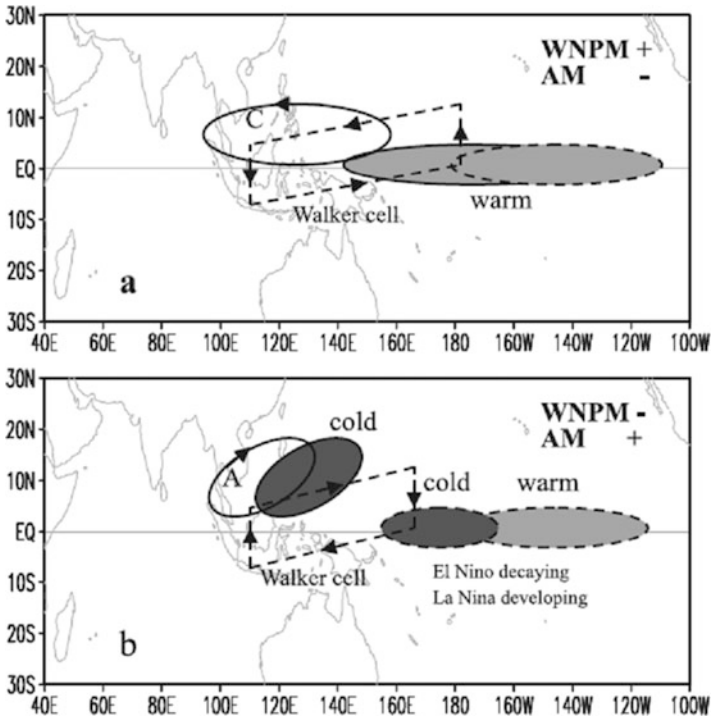

Fig. 6.24 Schematic diagrams showing the JJA (*solid line*) and DJF (*dashed line*) processes responsible for (**a**) out-of-phase relation from a strong WNPM to a weak AM and (**b**) out-of-phase relation from a weak WNPM to a strong AM (From Gu et al. (2010). © Copyright 2010 American Meteorological Society (AMS))

developing or La Niña decaying/El Niño Modoki developing events. For the first scenario, the remote forcing of the eastern Pacific SSTA holds a key. For example, a warm SSTA forces a Rossby wave response and low-level cyclonic shear over WNP (Gill 1980), which further enhances WNPM through the Ekman-pumping induced boundary layer convergence. As the SSTA continues to develop toward the boreal winter, the same sign of the SSTA weakens the AM through the anomalous Walker circulation in boreal winter. For the second scenario, the persistence of an anomalous anticyclone during the El Niño decaying phase holds a key in inducing a weak WNPM. As the decay of an El Niño is often accompanied with the onset of La Niña in the late year, the cold SSTA in the eastern Pacific may enhance AM in boreal winter through anomalous Walker circulation. Thus, the connection of WNPM and AM in the second scenario depends on both the persistence of the anomalous WNP anticyclone and the phase transition of the eastern Pacific SSTA (Fig. 6.24b).

The negative simultaneous correlation between WNPM and IM is mainly caused by the following two scenarios. The first scenario consists of the El Niño earlier onset (or La Niña persistence) events. The SSTA in the eastern Pacific, through

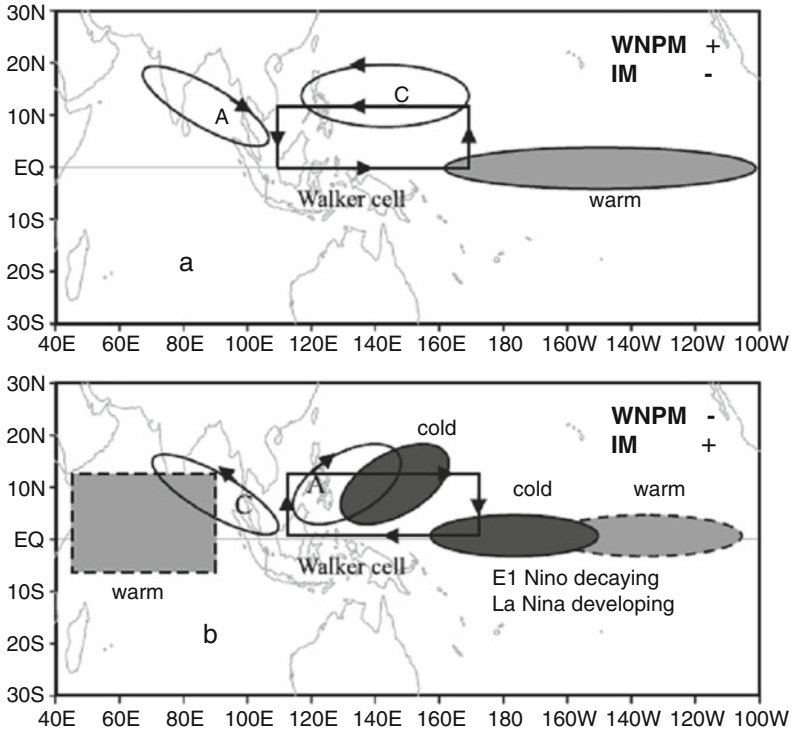

Fig. 6.25 Schematic diagrams showing the JJA (*solid line*) and DJF (*dashed line*) processes responsible for (**a**) simultaneous negative correlation between a strong WNPM and a weak IM and (**b**) simultaneous negative correlation between a weak WNPM and a strong IM (From Gu et al. (2010). © Copyright 2010 American Meteorological Society (AMS))

anomalous central equatorial heating, leads to the cyclonic wind shear in WNP and subsidence over the Maritime Continent. The former enhances the WNPM while the latter suppresses the IM (Fig. 6.25a). The second scenario consists of the El Niño decaying/La Niña developing (or La Niña decaying/El Niño developing) events. While a dry (wet) WNPM is attributed to the anomalous low-level anticyclone (cyclone) over WNP that persists from boreal winter to summer, a wet (dry) IM is caused by the eastern Pacific SSTA that has transitioned from a positive (negative) to a negative (positive) episode in JJA or by a basin-wide Indian Ocean warming (cooling) (Fig. 6.25b) that persists from El Niño (La Niña) mature winter to the subsequent summer. The basin-wide Indian Ocean warming may enhance (weaken) IM through increased (decreased) moisture transport (Chang and Li 2000; Li et al. 2001; Li and Zhang 2002).

Previous observational studies (e.g., Lau and Yang 1996; Li et al. 2001; Li and Zhang 2002) revealed that a warm SST anomaly in the tropical Indian Ocean leads a strong Indian monsoon. Chang and Li (2000) argued that the warm SSTA in Indian Ocean has both positive and negative effects on the Indian monsoon rainfall.

Table 6.2 Lagged correlation coefficients among WNPM, IM, and AM for 1979–2005 using GPCP2 and JRA data

From	***IM***	AM	***WNPM***	***AM***	***WNPM***
	JJA(0)	DJF(0)	***JJA(0)***	***DJF(0)***	***JJA(0)***
To	***AM***	IM	***AM***	***WNPM***	***IM***
	DJF(1)	JJA(0)	***DJF(1)***	***JJA(0)***	***JJA(0)***
Correlation coefficient	***0.35***	−0.26	***−0.32***	***0.32***	***−0.70***
Number of events	***17***	14	***14***	***18***	***15***

From Gu et al. (2010). © Copyright 2010 American Meteorological Society (AMS)
Note: The 90% (95%) significance level corresponds to a correlation coefficient of 0.32 (0.38). Number of events indicates the number of years during which the relationship between two monsoons is consistent with the correlation coefficient

A positive SST anomaly, on the one hand, increases the local surface humidity. The increased moisture may be further transported by the mean monsoon circulation, leading to a strong monsoon. On the other hand, the positive SSTA reduces the land–sea thermal contrast and thus decreases the monsoon rainfall. Both the scale analysis (Chang and Li 2000) and model simulations (e.g., Meehl and Arblaster 2002) showed that the positive effect is greater.

In analyzing the simultaneous IM-WNPM negative correlation, we notice a special case in summer 2001 that does not belong to both the scenarios above. As an anomalous cyclone persisted over SCS/WNP from winter to summer 2001 in association with the decay of a La Niña episode, no significant basin-wide SST anomalies appeared prior to the monsoon season in the tropical Indian Ocean, and by summer 2001, the tropical eastern Pacific SST became normal. Nevertheless, the IM was significantly weakened. The cause of the weak IM is possibly attributed to the atmospheric Rossby wave response to suppressed convection over the Maritime Continent, which, in turn, is caused by enhanced convective heating over the WNPM through the anomalous local Hadley cell (Kajikawa and Yasunari 2003). This implies that there might be a possible self-regulating process between the two sub-monsoon systems.

The composite analysis results above are based on the CMAP and NCEP Reanalysis 2 data. To examine the sensitivity of the aforementioned phase relationships to different data products, we conduct the same analysis procedure for two independent datasets. The first dataset includes GPCP2 rainfall and JRA reanalysis for the same period. The second dataset includes the PREC rainfall and NCEP/NCAR reanalysis for a longer period (1948–2006). Table 6.2 shows the lagged correlations among the three sub-monsoon systems using the GPCP/JRA dataset. It is found that the correlation coefficient between WNPM and the succeeding AM is −0.32, and the correlation coefficient between WNPM and the preceding AM is 0.32, both of which just pass the 90% significance level. The simultaneous correlation coefficient between WNPM and IM is −0.70, exceeding the 99% significant level.

The calculation of the longer record (1948–2006) dataset of NCEP/NCAR and PREC products (see Table 6.3) shows that the correlation coefficient between

Table 6.3 Lagged correlation coefficients among WNPM, IM, and AM for 1948–2006 using NECP/NCAR and PREC data

From	IM	AM	***WNPM***	AM	***WNPM***
	JJA(0)	DJF(0)	***JJA(0)***	DJF(0)	***JJA(0)***
To	AM	IM	***AM***	WNPM	***IM***
	DJF(1)	JJA(0)	***DJF(1)***	JJA(0)	***JJA(0)***
Correlation coefficient	0.21	−0.06	***−0.39***	0.07	***−0.29***
Number of events	36	36	***36***	34	***33***

From Gu et al. (2010). © Copyright 2010 American Meteorological Society (AMS)
Note: The 90% (95%) significance level corresponds to a correlation coefficient of 0.22 (0.26). Number of events indicates the number of years during which the relationship between two monsoons is consistent with the correlation coefficient

WNPM and the succeeding AM is −0.39, exceeding the 99% significance level. The simultaneous correlation coefficient between WNPM and IM is −0.29, exceeding the 95% significance level. The lagged correlation between AM and the succeeding WNPM, however, becomes insignificant. Thus, the three datasets point out in general a robust simultaneous IM-WNPM relation and a robust lagged phase relation between WNPM and the subsequent AM but a weak phase relation between AM and the subsequent WNPM. Thus, a caution is needed when a seasonal forecast is conducted based on the weak phase relationship.

A further analysis of the longer-record data reveals that the inter-monsoon relations are not stationary and they exhibit a marked interdecadal variation. For example, the significant negative correlation between WNPM and the succeeding AM appears at the beginning of 1960s, the mid-1970s, and after 1985. The significant negative simultaneous correlation between IM and WNPM occurs after 1975. The significant positive correlation between WNPM and the preceding AM appears from the end of 1960s to the beginning of 1970s. During other periods, the positive correlation is weak.

It is worth mentioning that the mechanisms discussed above are primarily based on the SSTA forcing. As we know, in addition to the lower boundary forcing, the monsoons are also influenced by internal atmospheric modes, such as synoptic and intraseasonal timescale motions.

6.8 Effect of Aerosol on Monsoon

Because of agriculture burning and burning fossil fuel, aerosol concentration in the troposphere increases rather steadily in the twentieth century (IPCC 2007). Anthropogenic aerosols absorb and scatter solar radiation and thus impose a negative radiative forcing to the earth surface ("dimming effect") (Meywerk and Ramanathan 1999; Ramanathan et al. 2005). Aerosols can also serve as cloud condensation nuclei and affect cloud formation, through which aerosols can also affect climate indirectly (Rosenfeld 2000; Rosenfeld et al. 2014). It has been

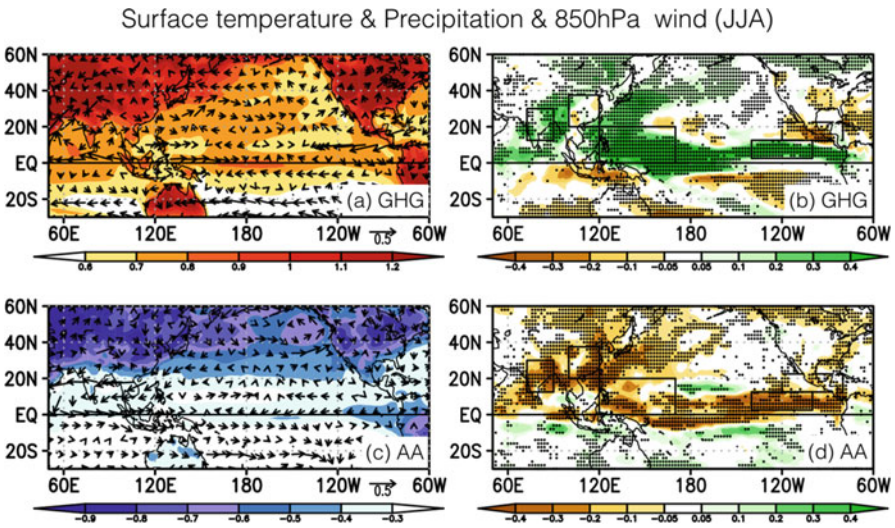

Fig. 6.26 Trends of surface temperature (shading, K century^{-1}) and 850 hPa winds (vector, m/s century^{-1}) during boreal summer over the period 1850–2005 are shown in left column and precipitation trends (shading, mm day^{-1} century^{-1}) in right column. (**a**) and (**b**) for results from greenhouse gas only experiments, (**c**) and (**d**) for the aerosol only experiments. Stippling denotes the regions where precipitation trends in at least 7 (out of 9) models agree with the sign of multi-model mean precipitation trends (From Zhang and Li (2016a). © Copyright 2016, American Geophysical Union (AGU))

reported that the radiative forcing of anthropogenic aerosols can be as large as that of anthropogenic greenhouse gases but with opposite sign, despite larger uncertainty (IPCC 2007).

However, unlike the anthropogenic greenhouse gases, the lifetime of anthropogenic aerosols is relatively short (Ramanathan et al. 2005). Consequently, aerosols concentrate and are thus more influential over the land area in the northern hemisphere (Li et al. 2015; Zhang and Li 2016a). As a result, the anthropogenic aerosols can significantly affect land–ocean thermal contrast, which is the main driver of the monsoon system (Guo et al. 2015; Salzmann et al. 2014). Indeed, it has been found that the East Asian summer monsoon rainfall has been weakening due to the substantial land cooling associated with the anthropogenic aerosols (Song et al. 2014). A prominent drying trend has also been found over the Indian summer monsoon region, which has been related to the anthropogenic aerosol effect as well (Bollasina et al. 2011; Li et al. 2015). Furthermore, the weakening of the Indian summer monsoon circulation has been attributed to the anthropogenic aerosol-induced interhemispheric cooling contrast, i.e., greater cooling in northern hemisphere (Bollasina et al. 2011).

Figure 6.26 shows single-forcing experiments from the Coupled Model Intercomparison Project Phase 5 (CMIP5) climate models that separate the effects of anthropogenic aerosols and greenhouse gases. It is clear that the anthropogenic aerosols induce prominent surface cooling anomalies over the northern hemisphere

during boreal summer, which consequently results in reduced land–ocean thermal contrast and weakened summer monsoon circulations. For instance, low-level easterly and northerly anomalies prevail over the Indian summer monsoon region, opposing the mean state southwesterlies (Fig. 6.26c). Similarly, the East Asian summer monsoon circulation is weakened due to the anthropogenic aerosol effect. The decreased moisture transport associated with these circulation changes induces drying anomalies over the Asian summer monsoon region (Fig. 6.26d). The inter-tropical convergence zone (ITCZ) over eastern tropical Pacific is also weakened associated with the anthropogenic aerosol-induced surface cooling anomalies. In addition to the dynamic effect, anthropogenic aerosol-induced cooling anomalies can also reduce the water vapor content and thus affect rainfall thermodynamically. This effect is important for driving the negative rainfall anomalies over the western North Pacific summer monsoon region.

In contrast to the anthropogenic aerosols, anthropogenic greenhouse gases tend to enhance rainfall by raising temperature and thus increasing moisture. As a result, both the Asian summer monsoon region and the ITCZ receive more rainfall due to the anthropogenic greenhouse gases (Fig. 6.26a). Note also that the land warming associated with anthropogenic greenhouse gases is apparently greater than that over the ocean surface, despite its relatively uniform distribution in the troposphere. This land–ocean warming contrast is a well-known feature that can be found in both observations and climate model simulations (Zhang and Li 2016b). As a result, the land–ocean thermal contrast is enhanced over the Asian summer monsoon region, which induces enhanced monsoon circulation over India that brings about more precipitation (Fig. 6.26a, b).

It is interesting to note that the East Asian summer monsoon circulation is not enhanced by the anthropogenic greenhouse gas effect, despite the greater land surface warming. This is in contrast to the weakened southwesterlies over East Asia when the land–ocean thermal contrast is reduced due to the aerosol effect (Fig. 6.26c). When forced with anthropogenic greenhouse gases, there is substantial positive rainfall anomaly over the western North Pacific summer monsoon region, which in turn drives low-level convergence anomaly that further enhances rainfall in situ ("richest-get-richer", Hsu and Li 2012). Since the East Asia and western North Pacific summer monsoon are dynamically connected, the circulation change over the western North Pacific will induce anomalous divergence over East Asia that reduces moisture transport and favors a drying anomaly. The combined dynamic and thermodynamic effect of the anthropogenic greenhouse gases leaves a small rainfall change over the East Asian summer monsoon region (Fig. 6.26b).

Hence, the two primary anthropogenic forcings act against each other over most regions. Note that the linear addition of the two single-forcing experiments reasonably reproduces the anomalies from the experiments in which the two forcing exist simultaneously (Fig. 6.27). Hence, these two forcing act mostly in a linear way. However, the relative importance of the two anthropogenic forcing is different over different regions. Overall, the thermodynamic effect of greenhouse gases is greater than that of aerosols due to the greater radiative forcing. Consequently, the rainfall changes over the western North Pacific summer monsoon region and the ITCZ over

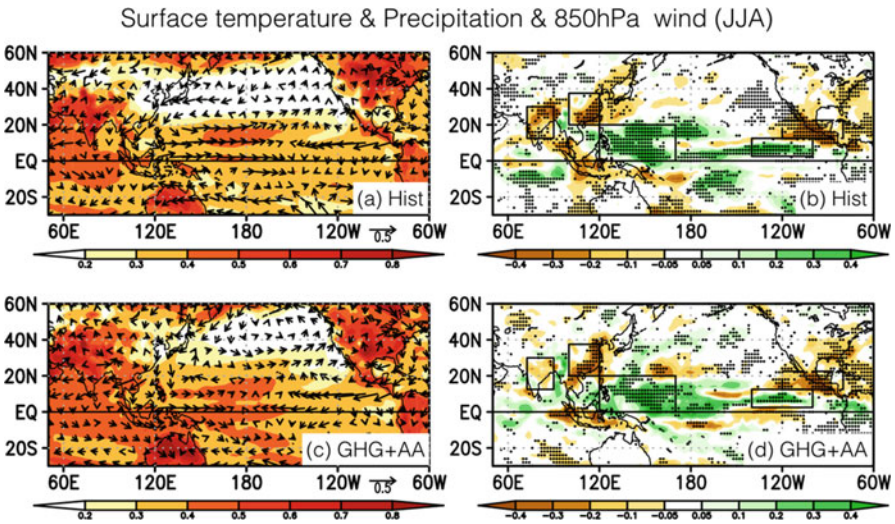

Fig. 6.27 Same as Fig. 6.1 but for results from total forcing experiments in (**a**) and (**b**), and the linear addition of results from greenhouse gas only and aerosol only experiments in (**c**) and (**d**) (Adapted from Zhang and Li (2016a). © Copyright 2016, American Geophysical Union (AGU))

eastern tropical Pacific are dominated by the greenhouse gas effect and thus positive. Over the land monsoon region, such as the Indian and East Asian summer monsoon region, the rainfall anomalies are negative, which is primarily associated with weakening of the monsoon circulation caused by reduced land–ocean thermal contrast associated with the aerosol effect (Fig. 6.27).

Questions

1. Through what physical processes does the El Niño exert a remote impact on the Indian summer monsoon?
2. Through what physical processes does the El Niño exert a remote impact on the East Asian summer monsoon? What is the key circulation system that connects El Niño and East Asian summer monsoon?
3. Through what processes does the anomalous anticyclone in WNP affect the Meiyu rainfall in East Asia?
4. What triggers and maintains the WNP anomalous anticyclone during El Niño developing and mature phases?
5. Through what processes does the tropical Indian Ocean SST anomaly influence the WNP circulation anomaly?
6. Why does the Indian Ocean basin warming become effective in influencing the WNP circulation anomaly only during El Niño decaying summer?
7. What is the relative role of tropical Indian Ocean basin warming and local cold SSTA in maintaining the anomalous anticyclone in WNP during El Niño decaying summer?

8. What is the phase relationship between the WNP monsoon and the Indian monsoon?
9. What is the tropospheric biennial oscillation (TBO)? What theories have been proposed to explain the TBO?
10. What causes the quasi-biennial and lower-frequency variability of the Indian summer monsoon precipitation?

References

Barnett TP (1991) The interaction of multiple time scales in the tropical climate system. J Clim 4:269–285

Bollasina MA, Ming Y, Ramaswamy V (2011) Anthropogenic aerosols and the weakening of the South Asian summer monsoon. Science 334:502–505. doi:10.1126/science.1204994

Chang C-P, Li T (2000) A theory for the tropical tropospheric biennial oscillation. J Atmos Sci 57:2209–2224

Chang C-P, Li T (2001) Nonlinear interactions between the TBO and ENSO. In: Chang CP et al (eds) East Asian and western Pacific meteorology and climate, World Scientific Series on Meteorology East Asia, vol 1. World Science, Singapore, pp 167–179

Chang C-P, Zhang Y, Li T (2000a) Interannual and interdecadal variations of the East Asian summer monsoon and tropical Pacific SSTs. Part I: Roles of the subtropical ridge. J Clim 13:4310–4325

Chang C-P, Zhang Y, Li T (2000b) Interannual and interdecadal variations of the East Asian summer monsoon and tropical Pacific SSTs. Part II: Meridional structure of the monsoon. J Clim 13:4326–4340

Chen TC, Weng SP, Yamazaki N, Kiehne S (1998) Interannual variation in the tropical cyclone formation over the western North Pacific. Mon Weather Rev 126:1080–1090

Chen J-M, Li T, Shih J (2007) Fall persistence barrier of SST in the South China Sea associated with ENSO. J Clim 20:158–172

Chen M, Li T, Shen X, Wu B (2016) Relative roles of dynamic and thermodynamic processes in causing evolution asymmetry between El Niño and La Niña. J Clim 29:2201–2220

Chiang JCH, Sobel AH (2002) Tropical tropospheric temperature variations caused by ENSO and their influence on the remote tropical climate. J Clim 15:2616–2631

Fu X, Wang B (2001) A coupled modeling study of the annual cycle of Pacific cold tongue. Part I: Simulation and sensitivity experiments. J Clim 14:765–779

Fu X, Wang B, Li T (2002) Impacts of air-sea coupling on the simulation of the mean Asian summer monsoon in the ECHAM4 model. Mon Weather Rev 130:2889–2904

Fu X, Wang B, Li T, McCreary J (2003) Coupling between northward propagating ISO and SST in the Indian Ocean. J Atmos Sci 60:1733–1753

Gaspar P (1988) Modeling the seasonal cycle of the upper ocean. J Phys Oceanogr 18:161–180

Gill AE (1980) Some simple solutions for heat-induced tropical circulation. Q J R Meterol Soc 106:447–462

Gill AE (1982) Atmosphere and ocean dynamics. Academic, New York

Gu D, Li T, Ji Z, Zheng B (2010) On the Western North Pacific Monsoon, Indian Monsoon and Australian Monsoon Phase Relations. J Clim 23:5572–5589

Guo L, Turner AG, Highwood EJ (2015) Impacts of 20th century aerosol emissions on the South Asian monsoon in the CMIP5 models. Atmos Chem Phys 15:6367–6378. doi:10.5194/acp-15-6367-2015

Hong C-C, Li T, Lin H, Chen Y-C (2010) Asymmetry of the Indian Ocean basin-wide SST anomalies: roles of ENSO and IOD. J Clim 23:3563–3576

Hsu P-C, Li T (2012) Is "rich-get-richer" valid for Indian Ocean and Atlantic ITCZ? Geophys Res Lett 39:L13705. doi:10.1029/2012gl052399
Huang R, Wu Y (1989) The influence of ENSO on the summer climate change in China and its mechanism. Adv Atmos Sci 6:21–32
IPCC, Climate Change (2007) The physical science basis. In: Solomon S et al (eds) Contribution of Working Group I to the fourth assessment report of the Intergovernmental Panel on Climate Change. Cambridge University Press, Cambridge/New York, 996 pp
Ju J, Slingo JM (1995) The Asian summer monsoon and ENSO. Q J R Meteorol Soc 121:1133–1168
Kajikawa Y, Yasunari T (2003) The role of the local Hadley circulation over the western Pacific on the zonally asymmetric anomalies over the Indian Ocean. J Meteorol Soc Jpn 81:259–276
Kawamura R (1998) A possible mechanism of the Asian summer monsoon-ENSO coupling. J Meteorol Soc Jpn 76:1009–1027
Klein SA, Soden BJ, Lau NC (1999) Remote sea surface temperature variations during ENSO: evidence for a tropical atmospheric bridge. J Clim 12:917–932
Lau N-C, Nath MJ (2003) Atmosphere–ocean variations in the Indo-Pacific sector during ENSO episodes. J Clim 16:3–20
Lau K-M, Sheu PJ (1988) Annual cycle, quasi-biennial oscillation, and southern oscillation in global precipitation. J Geophys Res 93:10975–10988
Lau K-M, Wu HT (2001) Principal modes of rainfall–SST variability of the Asian summer monsoon: a reassessment of the monsoon–ENSO relationship. J Clim 14:2880–2895
Lau K-M, Yang S (1996) The Asian monsoon and predictability of the tropical ocean-atmosphere system. Q J R Meteorol Soc 122:945–957
Li T (2006) Origin of the summertime synoptic-scale wave train in the western North Pacific. J Atmos Sci 63:1093–1102
Li T, Wang B (2005) A review on the western North Pacific monsoon: synoptic-to-interannual variabilities. Terr Atmos Ocean Sci 16:285–314
Li C, Yanai M (1996) The onset and interannual variability of the Asian summer monsoon in relation to land-sea thermal contrast. J Clim 9:358–375
Li T, Zhang Y (2002) Processes that determine the quasibiennial and lower-frequency variability of the South Asian monsoon. J Meteorol Soc Jpn 80:1149–1163
Li T, Zhang YS, Chang CP, Wang B (2001) On the relationship between Indian Ocean SST and Asian summer monsoon. Geophys Res Lett 28:2843–2846
Li T, Wang B, Chang CP, Zhang YS (2003) A theory for the Indian Ocean dipole-zonal mode. J Atmos Sci 60:2119–2135
Li T, Liu P, Fu X, Wang B, Meehl GA (2006) Spatiotemporal structures and mechanisms of the tropospheric biennial oscillation in the Indo-Pacific warm ocean regions. J Clim 19:3070–3087
Li X, Ting M, Li C, Henderson N (2015) Mechanisms of Asian summer monsoon changes in response to anthropogenic forcing in CMIP5 models. J Clim 28:4107–4125. doi:10.1175/JCLI-D-14-00559.1
Madden RA, Julian PR (1971) Detection of a 40–50 day oscillation in the zonal wind in the tropical Pacific. J Atmos Sci 28:702–708
Madden RA, Julian PR (1972) Description of global-scale circulation cells in the tropics with a 40–50 day period. J Atmos Sci 29:1109–1123
McCreary JP, Yu ZJ (1992) Equatorial dynamics in a 2.5-layer model. Prog Oceanogr 29:61–132
Meehl GA (1987) The annual cycle and interannual variability in the tropical Pacific and Indian Ocean regions. Mon Weather Rev 115:27–50
Meehl GA (1993) A coupled air-sea biennial mechanism in the tropical Indian and Pacific regions: role of the ocean. J Clim 6:31–41
Meehl GA (1994) Coupled land-ocean-atmosphere processes and south Asian monsoon variability. Science 266:263–267
Meehl GA (1997) The South Asian monsoon and the tropospheric biennial oscillation. J Clim 10:1921–1943

Meehl GA, Arblaster JM (2002) GCM sensitivity experiments for the Indian monsoon and tropospheric biennial oscillation transition conditions. J Clim 15:923–944
Meywerk J, Ramanathan V (1999) Observations of the spectral clear-sky aerosol forcing over the tropical Indian Ocean. J Geophys Res 104:24359–24370. doi:10.1029/1999JD900502
Mooley DA, Parthasarathy B (1984) Fluctuations in all- India summer monsoon rainfall during 1871–1978. Clim Chang 6:287–301
Mooley DA, Shukla J (1987) Variability and forecasting of the summer monsoon rainfall over India. In: Chang C-P, Krishnamurti TN (eds) Monsoon meteorology. Oxford University Press, New York, pp 26–59
Murakami M (1979) Large-scale aspects of deep convective activity over the GATE data. Mon Weather Rev 107:994–1013
Nicholls N (1978) Air-sea interaction and the quasi-biennial oscillation. Mon Weather Rev 106:1505–1508
Ramanathan V et al (2005) Atmospheric brown clouds: impacts on South Asian climate and hydrological cycle. Proc Natl Acad Sci **102**:5326–5333. doi:10.1073/pnas.0500656102
Rasmusson EM, Wang X-L, Ropelewski CF (1990) The biennial component of ENSO variability. J Mar Syst 1:71–96
Reynolds RW, Smith TM (1994) Improved global sea surface temperature analyses using optimum interpolation. J Clim 7:929–948
Rosenfeld D (2000) Suppression of rain and snow by urban and industrial air pollution. Science 287:1793–1796. doi:10.1126/science.287.5459.1793
Rosenfeld D, Sherwood S, Wood R, Donner L (2014) Climate effects of aerosol-cloud interactions. Science 343:379–380. doi:10.1126/science.1247490
Salzmann M, Weser H, Cherian R (2014) Robust response of Asian summer monsoon to anthropogenic aerosols in CMIP5 models. J Geophys Res Atmos 119, 11, 321–11, 337. doi:10.1002/2014JD021783
Shen S, Lau K-M (1995) Biennial oscillation associated with the East Asian summer monsoon and tropical Pacific sea surface temperatures. J Meteorol Soc Jpn 73:105–124
Soman MK, Slingo JM (1997) Sensitivity of the Asian summer monsoon-aspects of sea-surface-temperature anomalies in the tropical Pacific Ocean. Q J R Meteorol Soc 123:309–336
Song F, Zhou T, Qian Y (2014) Responses of East Asian summer monsoon to natural and anthropogenic forcings in the 17 latest CMIP5 models. Geophys Res Lett 41:596–603. doi:10.1002/2013GL058705
Sui C-H, Chung P-H, Li T (2007) Interannual and interdecadal variability of the summertime western North Pacific subtropical high. Geophys Res Lett 34:L11701
Tian SF, Yasunari T (1992) Time and space structure of interannual variations in summer rainfall over China. J Meteorol Soc Jpn 70:585–596
Tomita T, Yasunari T (1993) The two types of ENSO. J Meteorol Soc Jpn 71:273–284
Tomita T, Yasunari T (1996) Role of the northeast winter monsoon on the biennial oscillation of the ENSO/monsoon system. J Meteorol Soc Jpn 74:399–413
Walker GT (1923) Correlations in seasonal variations of weather. VIII, A further study of world weather. Mem Indian Meteorol Dept 24:75–131
Walker GT (1924) Correlations in seasonal variations of weather. VIII, A further study of world weather. Mem Indian Meteorol Dept 24:275–332
Wang B, Chan JC-L (2002) How strong ENSO regulates tropical storm activity over the western North Pacific. J Clim 15:1643–1658
Wang WC, Li K (1990) Precipitation fluctuation over semiarid region in northern China and the relationship with El Niño/southern oscillation. J Clim 3:769–783
Wang B, Li T (2004) East Asian monsoon-ENSO interactions. In: Chang CP et al (eds) East Asian and Western Pacific meteorology and climate, World Scientific Series Meteorology East Asia, vol 2. World Science, Singapore, pp 177–212
Wang B, LinHo (2002) Rainy seasons of the Asian-Pacific monsoon. J Clim 15:386–398

Wang B, Wu R (1997) Peculiar temporal structure of the South China Sea summer monsoon. Adv Atmos Sci 14:177–194
Wang B, Xie X (1996) Low-Frequency equatorial waves in vertically shear flow. Part I: Stable waves. J Atmos Sci 53:449–467
Wang B, Zhang Q (2002) Pacific–East Asian teleconnection, Part II: How the Philippine Sea anticyclone is established during El Niþo development. J Clim 15:3252–3265
Wang B, Li T, Chang P (1995) An intermediate model of the tropical Pacific ocean. J Phys Oceanogr 25:1599–1616
Wang B, Wu R, Fu X (2000) Pacific–East Asian teleconnection: How does ENSO affect East Asian climate? J Clim 13:1517–1536
Wang B, Clemons SC, Liu P (2003a) Contrasting the Indian and East Asian monsoons: implications on geologic timescales. Mar Geol 201:5–21
Wang B, Wu R, Li T (2003b) Atmosphere-warm ocean interaction and its impact on Asian-Australian Monsoon variation. J Clim 16:1195–1211
Webster PJ, Yang S (1992) Monsoon and ENSO: selectively interactive systems. Q J R Meteorol Soc 118:877–926
Webster PJ, Magana VO, Palmer TN, Shukla J, Tomas RA, Yanai M, Yasunari T (1998) Monsoons: processes, predictability, and the prospects for prediction. J Geophys Res 103:14451–14510
Wu B, Zhou T, Li T (2009) Seasonally evolving dominant interannual variability modes of East Asian climate. J Clim 22:2992–3005
Wu B, Li T, Zhou T (2010) Relative contributions of the Indian Ocean and local SST anomalies to the maintenance of the western North Pacific anomalous anticyclone during El Niño decaying summer. J Clim 23:2974–2986
Wu B, Zhou T, Li T (2012) Two distinct modes of tropical Indian Ocean precipitation in boreal winter and their impacts on equatorial western Pacific. J Clim 25:921–938
Xie A, Chung Y-S, Liu X, Ye Q (1998) The interannual variations of the summer monsoon onset over the South China Sea. Theor Appl Climatol 59:201–213
Xie S-P, Hu K, Hafner J, Tokinaga H, Du Y, Huang G, Sampe T (2009) Indian Ocean capacitor effect on Indo–western Pacific climate during the summer following El Niño. J Clim 22:730–747
Yanai M, Li C, Song Z (1992) Seasonal heating of the Tibetan Plateau and its effects on the evolution of the Asian summer monsoon. J Meteorol Soc Jpn 70:319–351
Yang S, Lau K-M (1998) Influences of sea surface temperature and ground wetness on Asian summer monsoon. J Clim 11:3230–3246
Yang S, Lau K-M, Sankar-Rao M (1996) Precursory signals associated with the interannual variability of the Asian summer monsoon. J Clim 9:949–964
Yasunari T (1990) Impact of the Indian monsoon on the coupled atmosphere/ocean system in the tropical Pacific. Meteorog Atmos Phys 44:29–41
Yasunari T (1991) The monsoon year—a new concept of the climatic year in the tropics. Bull Am Meteorol Soc 72:1331–1338
Yasunari T, Suppiah R (1988) Some problems on the interannual variability of Indonesian monsoon rainfall. In: Theon JS, Fugono N (eds) Tropical rainfall measurements. A. Deepak, Hampton, pp 113–122
Zhang L, Li T (2016a) Relative roles of anthropogenic aerosols and greenhouse gases in land and oceanic monsoon changes during past 156 years in CMIP5 models. Geophys Res Lett 43:5295–5301. doi:10.1002/2016GL069282
Zhang L, Li T (2016b) Relative roles of differential SST warming, uniform SST warming and land surface warming in determining the Walker circulation changes under global warming. Clim Dyn:1–11. doi:10.1007/s00382-016-3123-6
Zhang R, Sumi A, Kimoto M (1996) Impact of El Niño on the East Asian monsoon: a diagnostic study of the 86/87 and 91/92 events. J Meteorol Soc Jpn 74:49–62